

1 “Human displacements from tropical cyclone Idai attributable 2 to climate change”

3

4

5 Benedikt Mester ^{1 2}, Thomas Vogt ¹, Seth Bryant ^{2 3}, Christian Otto ¹, Katja Frieler ¹, and
6 Jacob Schewe ¹

7

8 ¹ Potsdam Institute for Climate Impact Research, Potsdam, Germany

9 ² Institute of Environmental Science and Geography, University of Potsdam, Potsdam,
10 Germany

11 ³ GFZ German Research Centre for Geosciences, Potsdam, Germany

12

13 Correspondence: Benedikt Mester (benedikt.mester@pik-potsdam.de)

14

15 Abstract

16 Extreme weather events, such as tropical cyclones, often trigger population displacement. The
17 frequency and intensity of tropical cyclones is affected by anthropogenic climate change.

18 However, the effect of historical climate change on displacement risk has so far not been
19 quantified. Here, we show how displacement can be partially attributed to climate change,
20 using the example of the 2019 tropical cyclone Idai in Mozambique. We estimate the
21 population exposed to high water levels following Idai’s landfall, using a combination of a 2D
22 hydrodynamical storm surge model and a flood depth estimation algorithm to determine inland
23 flood depths from remote sensing images, for factual (climate change) and counterfactual (no
24 climate change) mean sea level and maximum wind speed conditions. Our main estimates

25 indicate that climate change has increased displacement risk from this event by approximately
26 12,600 - 14,900 additional displaced persons, corresponding to about 2.7 to 3.2% of the

27 observed displacements. The isolated effect of wind speed intensification is double that of sea
28 level rise. These results are subject to important uncertainties related to both data and
29 modeling assumptions, and we perform multiple sensitivity experiments to assess the range
30 of uncertainty where possible. Besides highlighting the significant effects on humanitarian

31 conditions already imparted by climate change, our study provides a blueprint for event-based
32 displacement attribution.

33 1 Introduction

34 Between 1980 and 2021, an average of 45 tropical cyclones (TCs) globally have been
35 recorded per year (Guha-Sapir et al., 2022). TCs pose a set of societal risks to coastal
36 communities around the world. While related monetary losses are high, with an average of
37 US\$ 57.2 billion every year since 2008 (Guha-Sapir et al., 2022), TCs also displace an
38 average of 9.3 million people every year, with this hazard being responsible for 43% of all
39 weather-related displacements (IDMC, 2022). Such forced displacements are associated with
40 human suffering, as well as substantial financial costs (e.g., for providing shelter or from loss

Deleted:

Deleted:

Deleted: larger than

44 of economic production) and often require international assistance for disaster relief funds and
45 humanitarian response (Desai et al., 2021).

46
47 At the same time, global climate change is expected to alter TC characteristics, resulting in an
48 increase in overall TC intensity (maximum wind speed and precipitation) and hence in the
49 frequency of very intense TCs (category 4-5 on the Saffir-Simpson scale) (Knutson et al.,
50 2020). Primarily, this is the result of an increase in potential intensity due to warmer sea
51 surface temperatures (SST) (Emanuel, 2005, 2013, 1987). Sea level rise (SLR), also driven
52 by global warming, additionally compound coastal flood risk associated with TCs (e.g., Garner
53 Andra J. et al., 2017; Lin et al., 2012; Resio and Irish, 2016). Historic TC data records are
54 short and partially inconsistent, making it difficult to determine the degree of intensification
55 over time, despite observed changes in some basins, such as the South Indian Ocean
56 (Knutson et al., 2019; Kossin et al., 2013, 2007; Webster et al., 2005). Moreover, existing TC
57 datasets often focus on maximum wind speed, neglecting coastal and inland flooding which
58 may be the dominant hazards, e.g., as for Hurricane Katrina or Hurricane Harvey
59 (Bloemendaal et al., 2021). Paleo climate records (Lin et al., 2014; Nott and Hayne, 2001) and
60 synthetic TC tracks (Bloemendaal et al., 2022, 2020; Emanuel et al., 2006) can be used to
61 extend TC records. However, sediment availability is limited to a few coastal stretches and the
62 statistical resampling process incorporates only the average observed climatic conditions,
63 respectively, hampering the assessment of global climate change impacts over longer time
64 periods (Bloemendaal et al., 2020). Nonetheless, given that global mean surface air
65 temperature and sea level have already risen above pre-industrial conditions by about 1.1°C
66 and 0.20 m, respectively (Gulev et al., 2021), it is likely that recent TC landfalls have caused
67 more severe societal impacts than would be expected without climate change. A probabilistic
68 attribution addressing this topic is limited by the shortness of TC records (Trenberth et al.,
69 2015), and may be additionally affected by multi-decadal variability (e.g., the Atlantic
70 Multidecadal Oscillation) or interannual climate variability (e.g., the El Niño–Southern
71 Oscillation) (Patricola and Wehner, 2018). As a consequence, the portion of TC-induced
72 human displacements attributable to climate change has so far not been quantified.

73
74 In this study, we address this research gap for the particular case of displacement triggered
75 by TC Idai in 2019. We examine the floods in central Mozambique associated with TC Idai,
76 considered to be “one of the Southern Hemisphere’s most devastating storms on record”
77 (Warren, 2019). On the 14th of March, Idai made landfall near the densely populated port city
78 of Beira, inhabited by more than 530,000 people (Figure 1). Alongside strong winds (maximum
79 1-min sustained winds of 180 km/h) and extensive inland flooding caused by heavy rainfall,
80 the cyclone also created a storm surge of up to 4.4 m, leading to coastal flooding centered at
81 the port city of Beira (Probst and Annunziato, 2019). In Mozambique alone, TC Idai claimed
82 the lives of more than 600 people, and caused 478,000 internal displacements, as well as
83 widespread structural damage totaling more than US\$ 2.1 billion (Guha-Sapir et al., 2022;
84 IDMC, 2022).

85
86 Here, we investigate how the coastal flooding would have manifested in a counterfactual world
87 without climate change, and consequently, how many of the observed human displacements
88 from TC Idai can be linked to climate change. For the attribution of the impacts we follow the
89 storyline approach introduced by Shepherd (Shepherd, 2016). To this end, we account for two
90 known mechanisms through which global climate change could have affected coastal flood
91 hazard: SLR and amplification of storm intensity. Storm track and size are not changed, even

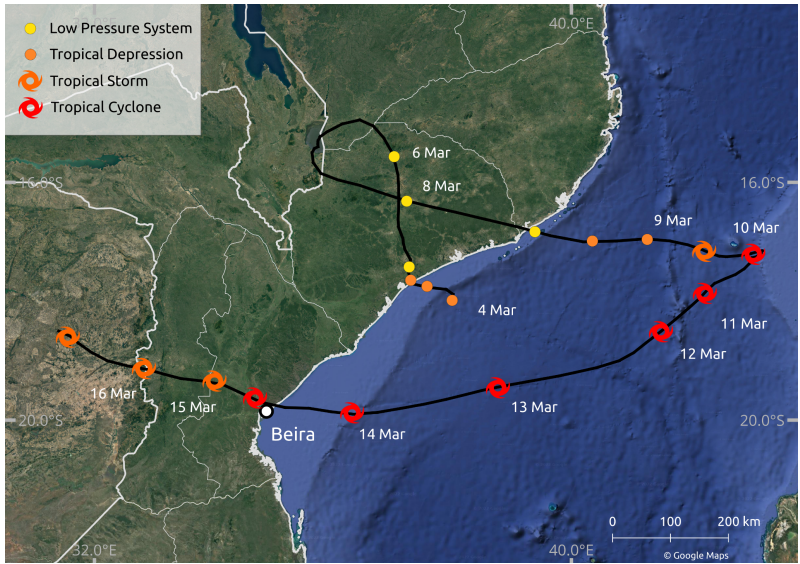
Deleted: of, fundamentally because

Deleted:

94 though both parameters are subject to the effects of climate change (Knutson et al., 2020,
95 2019). We first estimate the influence of climate change on sea level and TC intensity in the
96 South Indian Ocean. We employ a high-resolution hydrodynamic flood model to simulate TC
97 Idai's peak coastal flood extent and depth, both under historical conditions and under
98 counterfactual conditions with lower sea levels and lower maximum wind speed,
99 corresponding to a world without climate change. We additionally use satellite imagery to
100 account for inland (fluvial and pluvial) flooding, and estimate the total number of people
101 affected by flooding. We then model the number of displacements based on flood depth-
102 specific vulnerability factors, and estimate the fraction of displacements that can be attributed
103 to climate change by comparing results under factual vs. counterfactual conditions.
104

105 We use an estimate of SLR that attempts to separate natural variability in ice sheet and glacier
106 mass balance and retain only the long-term trend induced by global warming (Strauss et al.,
107 2021). Beyond this, however, our analysis is indifferent to whether the trends in sea level and
108 TC intensity are anthropogenic or not. This is in line with the definition of *impact attribution* put
109 forward by the Intergovernmental Panel on Climate Change (IPCC), where "changes in
110 natural, human, or managed systems are attributed to [a] change in [a] climate-related system"
111 (O'Neill et al., 2022). Such a question can be separated from the *climate attribution* question
112 of whether the change in the climate-related system - here, sea level and TCs - is due to
113 anthropogenic forcing. This separation allows us to focus on the link between climate change
114 and displacement despite remaining uncertainty about the exact anthropogenic contribution.
115 We will return to this issue in the discussion.
116

117 This study aims to attribute coastal-flood induced human displacements from TC Idai to
118 historic climate change, using a quantitative modeling approach. It addresses the need for
119 insights on the human impacts of climate change globally, and in particular in countries like
120 Mozambique that suffer from a combination of high exposure to climate-related hazards - in
121 this case, TCs - and high socio-economic vulnerability. Moreover, Mozambique, like many
122 other countries, is characterized by limited availability of in-situ observational data and a lack
123 of calibrated, local-scale inundation models. We use remote-sensing data and a globally
124 applicable modeling framework to characterize flood exposure during TC Idai; reported
125 displacement data is retrieved from the Global Internal Displacement Database (GIDD). Our
126 approach is thus transferable to other cases in virtually all relevant countries.
127
128
129
130
131
132
133



134
135
136
137
138
139
140

Figure 1: Trajectory of tropical cyclone Idai over the South Indian Ocean. Trajectory data is based on the IBTrACS database (Knapp et al., 2010). Mozambican administrative boundaries (GADM, 2018) in white; satellite image background by © Google Maps (Google Maps (a), 2022). Dates and tropical cyclone status adopted from ReliefWeb (ReliefWeb, 2019a).

141 2 Methods

142 2.1 Counterfactuals

143 Constructing counterfactuals for sea level and TC intensity requires estimating the effect of
144 historical climate change on these quantities. Total global mean sea level has risen by
145 approximately 230 mm since the turn of the 20th century (Church and White, 2011); at a rate
146 that has increased over time (Dangendorf Sönke et al., 2017). According to the IPCC, it is very
147 likely that the rate of global mean SLR was 1.5 (1.1 to 1.9) mm yr⁻¹ between 1902 and 2010,
148 and 3.6 (3.1 to 4.1) mm yr⁻¹ between 2006 and 2015 (Gulev et al., 2021). Nonetheless,
149 regional changes in sea level may differ substantially from the global average due to shifting
150 surface winds, the differential expansion of warming ocean water, and the addition of melting
151 ice, which can alter the ocean circulation (Fox-Kemper et al., 2021). Additionally, increases in
152 the amount of water stored on land (due to construction of dams and reservoirs), as well as
153 land subsidence, have also affected total sea level, with their relative effects varying
154 geographically (Church et al., 2004; Strauss et al., 2021).

155
156 Long-term in-situ observational records of SLR are scarce in the Indian Ocean (Han et al.,
157 2010), hampering a precise detection of changes in sea level. For example, no active tide

Deleted: c

159 gauge stations can be found on the coast of Beira (Beal et al., 2019), with the nearest station
160 located in Inhambane, Mozambique, 448 km south of Beira. However, regional historical SLR
161 rates for Mozambique, derived from satellite imagery or models, are close to global mean
162 estimates. IPCC rates of change in sea surface height (geocentric sea level) derived from
163 satellite altimetry show regional SLR off the coast of Mozambique at around 4.0 mm yr⁻¹ for
164 the period 1993–2012 (Church et al., 2013). Climate-induced SLR at the South-Eastern
165 African coastline (1993 - 2015) is estimated at ~3.5 mm yr⁻¹ using a coastal-length weighted
166 approach (Nicholls et al., 2021). Reconstructed sea level fields using global tide gauge data
167 suggests global-averaged SLR at 1.8 ± 0.3 mm yr⁻¹ over the 1950-2000 period, with regional
168 SLR off the coast of Mozambique at around 1.5 mm yr⁻¹ (Church et al., 2004). Han and
169 colleagues (Han et al., 2010) estimate regional Mozambican SLR at approximately 1.2 mm
170 yr⁻¹ between 1961-2008.

171
172 Given that these regional estimates are close to the global mean estimate by the IPCC, we
173 assume that total SLR near Beira is the same as the global mean, a comparable approach as
174 by Irish and colleagues (Irish et al., 2014). In order to exclude trends induced by natural
175 variability, particularly in sea level contributions from glaciers and ice sheets, we use estimates
176 of global mean sea level rise attributable to anthropogenic climate change for 1900–2012 from
177 Strauss and colleagues (Strauss et al., 2021). Their ensemble estimate is 6.6 to 17.1 cm,
178 which we use to define counterfactual sea level parameters for the coastal flood model. This
179 also implies assuming no substantial local effects of land subsidence and human-induced
180 changes in land water storage through reservoir construction and groundwater extraction that
181 would confound comparison with the global estimates. This is hard to verify, but can be
182 motivated by findings that city subsidence occurs only in a small fraction of the world's coasts
183 (Nicholls et al., 2021).

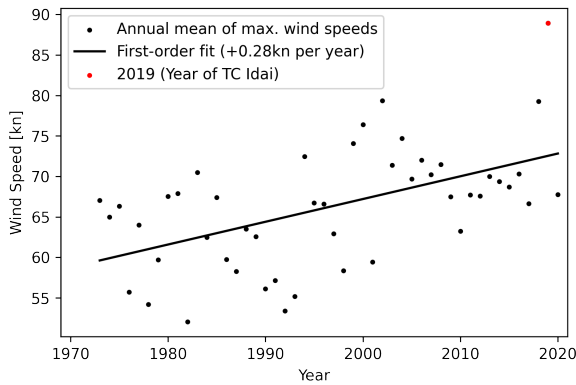
184
185 Tropical cyclones are projected to become more intense with rising temperatures (Knutson et
186 al., 2015), which is in line with the theoretical understanding of the potential intensity theory
187 (Emanuel, 1987). Observed TC wind speed data in the South Indian Ocean basin shows that
188 the maximum 10-minute sustained wind speed has been increasing by about 0.3 kn (0.15 m
189 s⁻¹) per year on average, over the period 1973-2019 (Figure 2). Prior to 1973, the rate of
190 increase was likely smaller, though observational data is lacking. We make a conservative
191 assumption corresponding to 50 years of increase at a rate of 0.2 kn (0.1 m s⁻¹) per year,
192 resulting in a total difference in maximum wind speed of approximately 10 kn (5.1 m s⁻¹). For
193 the case of TC Idai with maximum observed 10-minute sustained wind speeds of 105 kn (54
194 m s⁻¹), this corresponds to a 10% reduction in maximum wind speed by removing climate
195 change, which we adopt as a plausible assumption for counterfactual TC intensity.

196
197 This value is in line with the remote sensing-based estimates provided in Kossin et al. (2013),
198 who find that lifetime maximum TC intensities in the SIO have increased by about 4.6 m/s over
199 the period 1982-2009 (1.7 m/s per decade), which corresponds to 8.5% of TC Idai's maximum
200 intensity. If this rate of increase is linearly extrapolated to 2019, it results in an increase of
201 about 6.3 m/s (11.6%). Since the rate of increase has likely risen along with surface warming,
202 and since our period of reference extends back to 1973 rather than 1982, a value of 12% might
203 be a safer assumption for comparing the results of Kossin et al. (2013) with our own estimate.
204 To quantify the effect of uncertainty in the estimate of TC intensity change, we conduct two
205 sensitivity experiments, with counterfactual intensity lower than factual by 8.5% and 12%,

Deleted: ¶
¶

208 respectively, reflecting the SOI estimate of Kossin et al (2013) both directly and when
209 extrapolated for comparability with our own estimate.

210
211 We note that lower rates of change have been found in climate model-based studies. Knutson
212 et al. (2020) find a 6% increase in maximum intensity of SIO TCs per 2°C global mean surface
213 warming. When applied to the historical increase in global mean surface temperatures of
214 1.1°C, this would yield an increase of 3.3%. While these climate model estimates are important
215 both for assessing future changes and for understanding the underlying mechanisms of
216 observed trends, the remote-sensing based trend estimates are more relevant for informing
217 the construction of the counterfactual in our study.
218



219
220 **Figure 2: Annual means of maximum TC wind speeds in the South Indian Ocean**
221 **(maximum 10-minute sustained wind speeds).** Linear trend over the period 1973-2020;
222 data from IBTrACS database (Knapp et al., 2010).

223 2.2 Coastal Flood Modeling

224 The storm surge flood simulations are generated using the open-source geophysical flow
225 solver GeoClaw (Mandli and Dawson, 2014). GeoClaw uses an efficient adaptive mesh
226 refinement to model wind- and pressure-induced wave dynamics in the 2-dimensional depth-
227 averaged shallow water equations. The input data includes TC tracks, astronomical tides, and
228 topographical raster data (see below) and GeoClaw provides outputs in the form of gridded
229 maps of maximum flood heights as well as the temporal dynamics of storm surge at virtual
230 tide gauge locations. We configure GeoClaw to limit the automatic mesh refinement to a
231 spatial resolution of between 1 and 8 arc-seconds (approximately 30 and 240 m) inside of
232 Idai's landfall area and to between 100 and 900 arc-seconds (approximately 3 and 27 km) in
233 the open ocean.

234
235 As the factual input for GeoClaw, the TC track data from IBTrACS (Knapp et al., 2010)
236 provided by the WMO Regional Specialised Meteorological Center at La Reunion (operated

237 by MeteoFrance) is used. For the counterfactual scenarios with modified TC intensity, we
238 multiply all wind speed values along the track by a scalar factor of 0.9 (for a decrease of 10%
239 in intensity). The central pressure at each track position is increased by 0.1 times the
240 difference between central pressure and environmental pressure.

241
242 From the wind speed, pressure, and radius information provided along the TC track, GeoClaw
243 derives surface wind speeds and air pressure at arbitrary locations in space and time using a
244 radially symmetric wind profile (Holland, 1980) combined with the influence from the storm's
245 translational speed.

246
247 GeoClaw does not incorporate any tidal dynamics, nor meteorological forcings apart from the
248 TC wind and pressure fields mentioned above. To account for the influence of astronomical
249 tides, we configure GeoClaw to use an initial sea level according to gridded satellite altimetry
250 for 2019 (CMEMS, 2021), optionally enhanced by the minimum, mean, or maximum simulated
251 astronomical tides in the region of landfall according to the FES2014 global ocean tide atlas
252 (Lyard et al., 2021). For the counterfactual sea level scenarios, the amount of sea level rise
253 specified in the scenario description (between 6.5 and 17.0 cm) is subtracted from the initial
254 sea level.

255
256 The topographical input for GeoClaw is taken from digital elevation models (DEMs). We use
257 a combination of CoastalDEM 2.1 (Kulp and Strauss, 2021, 2018) in coastal areas, SRTM 15+
258 V2.3 (Tozer et al., 2019) over the open ocean and Multi-Error-Removed Improved-Terrain
259 (MERIT) DEM (Yamazaki et al., 2019) everywhere else. All datasets are converted to the
260 same geoidal vertical datum (EGM96) at a spatial resolution of 9 arc-seconds (approximately
261 300 m). This resolution is the highest resolution where we were able to obtain numerically
262 stable results from GeoClaw. We note that no harmonization has been applied to make up for
263 disagreements between the different DEM products so that the transition from CoastalDEM
264 topography to SRTM 15+ bathymetry can be steep.

265
266 Due to a lack of tide gauges or suitable observed flood extent in Mozambique, it is not possible
267 to validate the performance of GeoClaw for TC Idai in the factual model runs. However, we
268 compare the water levels at a virtual tide gauge station off the coast of Beira, where the highest
269 impacts from TC Idai have been reported, with simulated water levels from the Global Tide
270 and Surge Model (GTSM) (Dullaart et al., 2021; Muis et al., 2020), and find the best agreement
271 of maximum surge heights for the GeoClaw run with the maximum astronomical tide
272 assumption, closely followed by the run assuming the monthly mean sea level (no tidal
273 adjustment) (Supplementary Figure S1).

274 2.3 Inland Flood Depth Estimation

275 Gridded depth maximums for the flood event (Supplementary Figure S2) is calculated using
276 the Rolling HAND Inundation Corrected Depth Estimator (RICorDE) tool (Bryant et al., 2022)
277 supplied with terrain data from the MERIT DEM project, permanent surface water data from
278 the Joint Research Centre (JRC) Global Surface Water project (Pekel et al., 2016), and flood
279 extents from the FloodScan product (Atmospheric and Environmental Research & African Risk
280 Capacity, 2022). MERIT DEM provides a roughly 90 m resolution global layer derived from
281 multiple space-based sensors to minimize elevation errors. The maximum water extent layer

282 from JRC's Global Surface Water project provides a roughly 30 m resolution global layer of
283 locations detected as inundated on Landsat imagery (Wulder et al., 2016) from 1984-2019
284 (Pekel et al., 2016). Observed flood extents for TC Idai are obtained from Atmospheric and
285 Environmental Research & African Risk Capacity's accumulated 2-tier standard flood extent
286 depiction FloodScan product from 2019-03-01 to 2019-03-31 using the MERIT DEM
287 resolution. Originally developed for applications in Africa, this FloodScan algorithm relies on
288 satellite based low-resolution passive microwave data and was designed to capture national-
289 scale events. To accomplish this, the algorithm minimizes false-positives, making the
290 algorithm more prone to false-negatives and less sensitive to events with smaller spatial extent
291 and urban floods (Galantowicz and Picton, 2021). All data layers are re-projected to 90 m
292 resolution geodetic coordinates prior to the RICorDE computation.

293
294 RICorDE is a tool developed in pyQGIS for post-event analysis of fluvial flood events using
295 inundation masks derived from space-based observations. RICorDE first generates a Height
296 Above Nearest Drainage (HAND) grid followed by an inundation correction phase and a water
297 surface level (WSL) calculation phase. As part of pre-processing, the HAND grid is obtained
298 using WhiteboxTools' *ElevationAboveStream* (Lindsay, 2014) from the permanent surface
299 water layer and the DEM. In the first phase of RICorDE, the observed flood extents are
300 hydraulically corrected to account for under-predictions using the permanent surface water
301 layer and over-predictions using a HAND-derived inundation representing the upper quartile
302 of possible flooding extents. In the second phase, HAND values sampled from the inundation
303 shoreline are used to produce an interpolated WSL grid using WhiteboxTools' *CostAllocation*
304 algorithm (Lindsay, 2014). Finally, gridded water depths are obtained from this WSL grid
305 through subtraction with the DEM. RICorDE is explained in detail in the tool publication (Bryant
306 et al., 2022) and the source code can be accessed online
307 (<https://github.com/NRCan/RICorDE/tree/main>).

Deleted: https://github.com/cefect/RICorDE_pub

308
309 The slower, more complex RICorDE algorithm has been shown to produce more accurate
310 depths maps for two fluvial flood events in Canada when compared to faster, more disaster
311 response-focused solutions like the Floodwater Depth Estimation Tool (FwDET) (Bryant et al.,
312 2022; Cohen et al., 2018). While no data is available to validate the performance of the depths
313 estimate for TC Idai, visual inspection suggests results are less accurate in areas with higher
314 elevation (>20 m), especially where drainageways are of comparable width to the resolution
315 of the JRC water extent layer. These false negatives in the JRC layer propagate as positive
316 bias in the HAND routine, which leads to higher elevation water surface predictions and similar
317 positive bias in the depth values (see white arrow in Figure S3a).

318 2.4 Combined Flood Depth Product

319 The inland flood depth estimates from RICorDE are resampled from 3 arcsec to 9 arcsec,
320 using the average resampling method (Rasterio library for Python), to match the resolution of
321 the GeoClaw output. All flood depths are rounded to the nearest decimeter, their outline is
322 cropped to the area of interest, and the final factual flood depth in each grid cell (shown in
323 Figure 3a) is determined as the maximum of both products. This accounts for both potentially
324 partly obscured satellite imagery by clouds and potential underestimation by the numerical
325 model.
326

328
$$d_0 = \max (d_{c,0} , d_r) \quad (1)$$

329

330 with d_0 referring to the factual flood depth, and indices c and r referring to the coastal flood
331 model (GeoClaw) and to the remote sensing data translated into flood depth using RICorDE,
332 respectively. To derive the counterfactual flood depth d_{cf} , we subtract the difference between
333 modeled factual and counterfactual coastal flood depths from the combined factual flood
334 depth:

335

336
$$d_{cf} = d_0 - (d_{c,0} - d_{c,cf}) \quad (2)$$

337

338 2.5 Displacement

339 We use displacement data from the publicly accessible GIDD, maintained by the *Internal*
340 *Displacement Monitoring Centre* (IDMC, 2022). IDMC follows the definition of displacement
341 provided in the *Guiding Principles on Internal Displacement* (OCHA, 2004), which states that
342 “[i]nternally displaced persons are persons or groups of persons who have been forced or
343 obliged to flee or to leave their homes or places of habitual residence, ... and who have not
344 crossed an internationally recognized State border”. This definition covers permanent
345 displacement, temporary displacement, and pre-emptive evacuations (Gemenne, 2011), all
346 summarized as “displacements” within our study. No granular information is available in GIDD
347 on the type of displacement. Displacement numbers are based on multiple secondary sources,
348 such as IOM, OCHA, or - in the case of TC Idai - the Mozambique National Institute of Disaster
349 Management. The TC Idai event is categorized as a “storm” event, however, no information is
350 given on how many of the displacements were caused respectively by flooding, strong winds,
351 or a combination of both. Because of the extensive flooding observed in the wake of Idai’s
352 landfall and humanitarian reports often focused on flooding (ReliefWeb, 2019a), we assume
353 in our main analysis that all displacements are caused by flooding (either coastal or inland).
354 We assume that people exposed to flood levels greater or equal than 100 cm are affected by
355 the flooding and thus prone to displacement, following previous studies (Custer and Nishijima,
356 2015; Kam et al., 2021). However, we also test the sensitivity of our results to this threshold
357 choice by evaluating alternative water level thresholds of 10 cm and 50 cm. Our modeling
358 approach assumes an artificially deterministic link between the TC hazard and displacement,
359 which is adequate in the context of the factual-counterfactual approach where only one
360 parameter - storm surge hazard - is modified while everything else, including vulnerability, is
361 held constant. In general, the relationship between climatic events, pre-existing socio-
362 economic conditions, and displacement is complex and only partially understood (Cattaneo et
363 al., 2019; UK Government Office for Science, 2011). In other words, our study addresses the
364 question of how many displacements might have occurred in a different climate but with the
365 same vulnerability as observed; it does not address the question of how this vulnerability came
366 about.

367

368 We first determine the flood extent with depths greater than the selected water level threshold
369 and overlay it with population data to estimate the number of people affected. We use gridded
370 population data from GHS-POP (Schiavina et al., 2019) for the year 2015, on 9 arcsec
371 resolution. Population growth in Mozambique was 1.12 % between 2015 and 2019 (The World

372 Bank, 2022); we hence multiply all population grid cells with this factor, assuming a spatially
373 equal population growth.

374
375 We then calculate the ratio between the number of observed displacements, and the number
376 of affected people from the factual flood estimate. This ratio, which may be thought of as an
377 event-specific displacement vulnerability factor, is different for every tide assumption,
378 reflecting the uncertainty about the actual flood extent and depth. We compute for every
379 impact level threshold i and tide assumption h a displacement vulnerability factor $v_{i,h}$ by
380 dividing the number of observed displacements D_o by the total number of affected people of
381 the factual scenario $A_{i,h,o}$:

382
383
$$v_{i,h} = \frac{D_o}{A_{i,h,o}} \quad (3)$$

384
385 Multiplying the specific displacement vulnerabilities with the counterfactual numbers of
386 affected people, we derive the number of people at risk of displacement in a world without
387 climate change. This means that the difference between factual and counterfactual
388 displacement estimates comes only from differences in the flood hazard, while exposure and
389 vulnerability factors are held fixed. We achieve this by multiplying $v_{i,t}$ with the number of
390 affected people of the counterfactuals $A_{i,h,cf}$, and estimate the expected number of
391 displacements for each counterfactual scenario $D_{i,h,cf}$.

392
393
$$D_{i,h,cf} = v_{i,h} * A_{i,h,cf} \quad (4)$$

394
395 We point out that the use of predefined flood thresholds implies the assumption that at a given
396 flood depth, the risk of severe damages to, or even destruction of, residential buildings and
397 other infrastructure typically becomes so large that people *may* be forced to flee. The number
398 of people that *actually* become displaced then depends on additional physical, political and
399 socio-economic factors, which may vary between local contexts and are not generally known.
400 Their aggregate effect is reflected in the specific vulnerability factor $v_{i,h}$. In other words, the link
401 between flood hazard and displacement is “soft” in the sense that it is mediated by the local
402 vulnerability. An alternative assumption would be that there is an (event-specific) flood-depth
403 threshold below which there is no displacement, and above which people become displaced
404 regardless; that is, a “hard” link between flood hazard and displacement. In this case, the
405 flood-depth threshold could be derived directly from the data, as the depth level at which the
406 calculated number of affected people equals the reported number of displacements. When we
407 sum up the affected people per 10 cm flood depth increment for TC Idai, we obtain a threshold
408 of about 400 cm (similar for all tide assumptions; Supplementary Table S1), for which the
409 modeled number of affected people approximately equals the number of observed
410 displacements. This value is very high in comparison with the thresholds cited further above,
411 and we believe it is implausible for displacement to occur only in locations inundated by 4
412 meters or more. This exercise therefore lends further justification for the “soft link” approach.

413
414 Even though disaster reports for TC Idai suggest flooding to be the main driver of
415 displacement, high wind speeds may have locally intensified the impact of TC Idai (Figure S4)
416 and be partially responsible for the observed displacements. We conduct an additional
417 analysis where we assume that people affected by either flooding or wind (or both) were at
418 risk of displacement with an equal vulnerability factor. We use a wind speed threshold of 96

Deleted: ¶

420 kn (50 m s^{-1}) for population exposure (Geiger et al., 2018), corresponding to the Saffir–
421 Simpson scale classification 3 (major hurricane). The resulting wind field is overlaid with
422 gridded population data to compute the number of affected people, excluding those who are
423 already affected by flooding.

424 3 Results

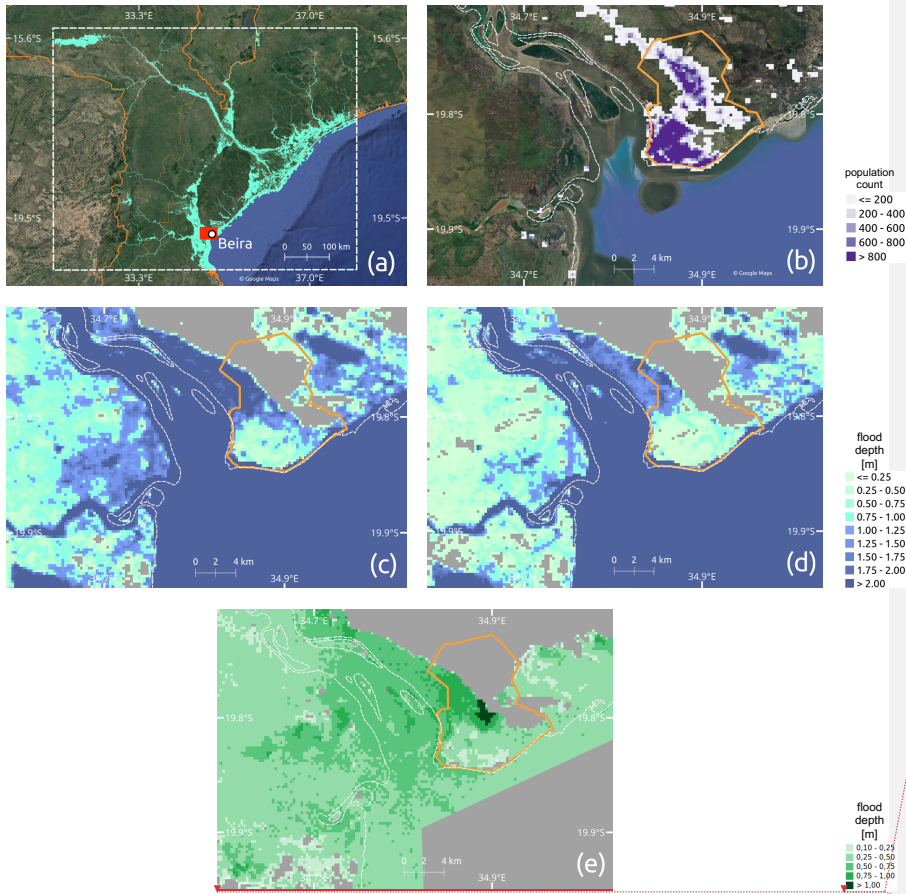
425 3.1 Simulated flooding

426 We calculate storm surge flood extent and depth for the factual (driven with observed wind
427 speeds and sea levels) and counterfactual (reduced wind speeds and sea level) scenarios.
428 The difference between factual and counterfactual flooding (maximum tide, 10.5 cm SLR, 10%
429 TC intensification) is illustrated in the densely populated area of Beira (Figure 3b), the city
430 where TC Idai made landfall and destroyed 90% of all houses according to some disaster
431 reports (ReliefWeb, 2019b). Beira consists of two major population centers, of which the
432 southern one is close to the seaside and exhibits a higher population count.

433
434 Both factual and counterfactual flood extent covers the southern, highly populated part of Beira
435 (Figure 3c and 3d). The northern parts of the city are only marginally affected. Flood extents
436 are also similar between factual and counterfactual simulations in the areas east of Beira and
437 around the inflow of the Buzi River, located on the opposite side of the bay. Only a few isolated
438 locations no longer experience flooding after removing the effects of climate change.

439
440 In contrast, differences in simulated flood depth are more pronounced (Figure 3e).
441 Counterfactual flood depths are up to 80 cm lower than factual flood depth in some parts of
442 the southern city center. The highest difference in flood depth, of up to 140 cm, is found
443 between the northern and southern population centers of Beira. Flood depth differences
444 outside of Beira are rather low, however, Figure 3c and 3d show that absolute flood depths
445 drop below the critical flood depth of 100 cm over great parts around the west bank of the
446 Pungwe River inflow. Overall, it is observable that depth differences (between factual and
447 counterfactual simulations) are higher in less populated parts, especially in Beira. This could
448 partly result from the fact that digital elevation models tend to overestimate elevation in dense
449 urban settings (Shen et al., 2019), thereby underestimating flood depth and potentially also
450 differences in flood depth between different scenarios, however, this is hard to ascertain given
451 the available data. Nonetheless, local variations in simulated flood depth should be interpreted
452 with care.

453
454
455
456
457
458
459



460
 461 **Figure 3: Simulated flood extent for Mozambique; population distribution and**
 462 **inundation levels for the greater area of Beira.** (a) Combined factual estimate of inland and
 463 coastal flooding (binary; flood/no-flood). White dashed box shows the area of interest in which
 464 flood exposure is computed. Red rectangle shows the extent of the section displayed in panel
 465 (b) - (e). (b) Population distribution for the greater area of Beira. Flood extent and levels for (c)
 466 the factual scenario (max. tide), and (d) the “counterfactual TC intensity + sea level rise (10.5
 467 cm) - max. tide” scenario. Flood depth difference between (c) and (d) is displayed in (e). City
 468 neighborhoods of Beira (HDX, 2019) are indicated by orange lines and shoreline (Wessel and
 469 Smith, 1996) is represented by dashed white lines in (b) - (e); satellite image background by
 470 © Google Maps (Google Maps (b), 2022) in (a) and (b).
 471

472 **3.2 Displacement**

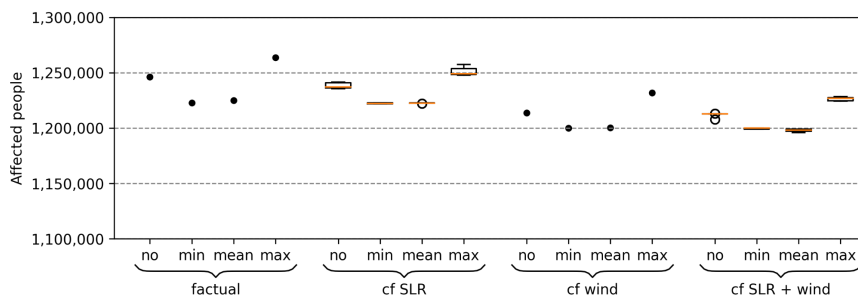
473 In the next step, we investigate how the factual and counterfactual flood estimates translate
 474 into population at risk of displacement for the whole of Mozambique. We compare factual and

477 counterfactual affected people/displacements and compute the absolute relative change
478 based on the counterfactual results, representing the increase in impact due to climate
479 change. Our analysis shows that the intensification of TC wind speeds leads to an increase in
480 flood affected people and, consequently, in displacements by up to 2.7%, while
481 counterfactuals regarding the sea level lead to only small changes by up to 1.3 % (Figure 4,
482 Table 1 and Table S2). A combination of both counterfactuals only slightly exceeds the range
483 (increase by up to 3.2% for the maximum tide assumption) as in contrast when considering
484 the TC intensification alone. Despite the large uncertainty regarding SLR since 1900, the
485 difference in the number of people affected (or displaced) is rather marginal; being less than
486 1% increase between the largest and the smallest SLR estimate for the “cf SLR” simulations.
487 Our results highlight that the tide assumption plays a major role. The minimum and mean tide
488 lead to marginal changes in affected/displaced people, in contrast to the maximum
489 astronomical tide and monthly mean sea level from satellite altimetry (no tide), which show for
490 the “cf SLR + wind” simulations a median change in 3.0% (maximum change in 3.2%) and
491 2.7% (3.2%), respectively. Given the high number of affected people, already small changes
492 in the counterfactual scenarios lead to high changes in absolute numbers. The coupled effect
493 of higher wind speeds and higher sea level increases the number of affected people and
494 displacements by up to 39,300 and 14,900 (maximum tide) and 38,100 and 14,600 (monthly
495 mean), respectively. Results regarding impact flood levels of 10 cm and 50 cm are displayed
496 in Table 1 and the supplementary material (Figure S5 and S6), showing even higher changes
497 for the counterfactual scenarios of up to 56,500 displacements (13.4% increase).
498

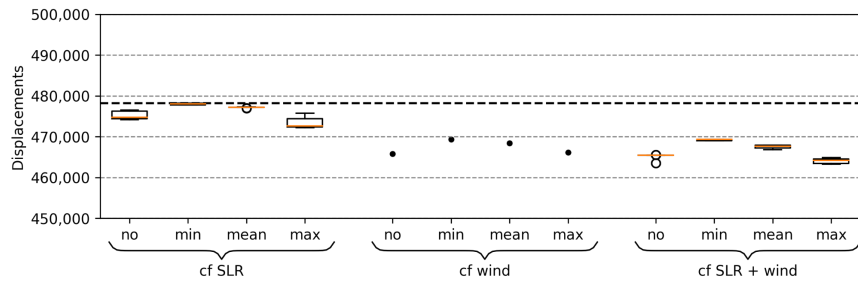
499 Besides our central TC intensification assumption of 10%, we also examine two alternative
500 assumptions of 8.5% and 12% intensification, respectively, for the “max” tide (Figure 5). The
501 spread among the intensification scenarios is rather small, with median relative changes
502 varying between 2.9% and 3.7%. This translates to median estimates of 35,300 and 44,600
503 affected people, or 13,400 and 16,900 displacements, respectively (Table 1 and Table S2). In
504 contrast, the difference between the highest (4.0%) and lowest values (2.2%) is larger. In
505 absolute terms, this means a range of between approximately 27,400 and 48,200 affected
506 people, or 10,400 and 18,200 displacements.
507

508 We assume that high wind speed caused only a marginal fraction of displacements, following
509 disaster reports, media coverage and experience from other events; as an extreme example,
510 wind by Hurricane Sandy caused less than 0.01% of the overall damage (Strauss et al., 2021).
511 Nonetheless, in an additional sensitivity analysis, we also account for the number of people
512 affected by high TC wind speeds of 50 m s^{-1} or above (Sect. Methods). Our analysis reveals
513 that the number of people affected not by flooding (maximum tide assumption, 100 cm impact
514 threshold) but by high wind speeds ranges between 340,900 to 360,600 in the factual
515 simulation. In the counterfactual, even the maximum wind speed attained in any grid cell
516 outside the flooded area drops from 51.5 m s^{-1} to 46.3 m s^{-1} , i.e. below the above-mentioned
517 threshold; thus, no people are counted as affected. Assuming the same vulnerability factor
518 for displacement due to high wind speed as due to flooding yields 103,700 to 112,100
519 displacements, or 21.7 to 23.4% of the total displacement, attributable to climate change.
520

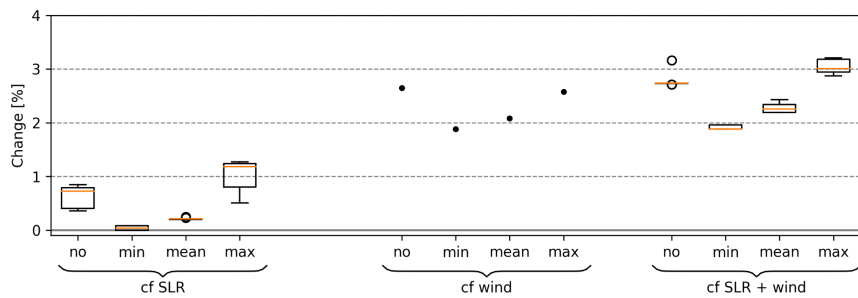
521
522
523



524



525



526

527

528

529

530

531

532

533

534

Figure 4: Simulated affected people (top), displacements (middle) and percentage change (bottom) for the 100 cm impact threshold. The percentage change compares factual and counterfactual displacements, and represents the absolute relative change based on the counterfactual results. Three counterfactual scenarios are shown: lower sea level (“cf SLR”), intensification (“cf wind”), and a combination of both (“cf SLR + wind”). Additionally, a variety of counterfactual sea levels as well as a set of astronomical tides is presented, covering minimum (“min”), mean (“mean”), and maximum (“max”) as well as monthly mean sea level from satellite altimetry (“no”). Bold dashed line in the middle panel shows the number of

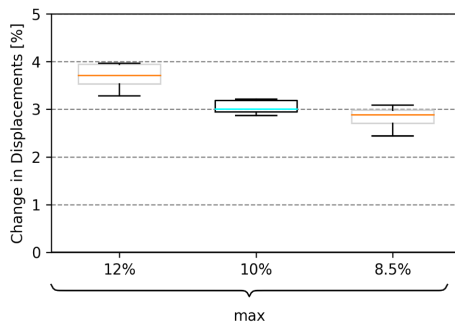
535 observed displacements. Percentile changes in affected people and displacements are the
 536 same. The second quartile Q2 (median) of the box plot is shown in orange, “whiskers” are
 537 placed at $\pm 1.5 \cdot$ interquartile range (Q3-Q1).
 538

539 **Table 1: Overview main results for modeled displacement impact.** Min./Median/Max. are
 540 related to the SLR scenarios. Orange background of the first results row indicates the primary
 541 parameter estimate. Cells with gray background indicate the altered parameter in comparison
 542 with the primary estimate.
 543

Counterfactual	Flood_Depth Threshold [cm]	Intensification [%]	Tide	Displacements Dif. Min.	Displacements Dif. Median	Displacements Dif. Max	Displacements Dif. Min. [%]	Displacements Dif. Median [%]	Displacements Dif. Max [%]
SLR + wind	100	10	max	13331	13958	14875	2.9	3.0	3.2
SLR + wind	100	10	no	12620	12740	14629	2.7	2.7	3.2
SLR + wind	100	10	min	8822	8822	9183	1.9	1.9	2.0
SLR + wind	100	10	mean	10235	10543	11353	2.2	2.3	2.4
SLR + wind	50	10	max	46695	49336	52275	10.8	11.5	12.3
SLR + wind	10	10	max	28557	32218	34456	6.4	7.2	7.8
SLR	100	10	max	2407	5584	5981	0.5	1.2	1.3
wind	100	10	max	-	12033	-	-	2.6	-
SLR + wind	100	8.5	max	10384	13354	14321	2.2	2.9	3.1
SLR + wind	100	12	max	14297	16870	18232	3.1	3.7	4.0

Deleted:

544



545

546 **Figure 5: Percentage change in displacements between factual and counterfactual, for**
 547 **three different TC intensification assumptions.** The percentage change compares factual
 548 and counterfactual displacements, and represents the absolute relative change based on the
 549 counterfactual results. The combined counterfactual scenario (“cf SLR + wind”) with 100 cm
 550 impact threshold and the maximum astronomical tide (“max”) is displayed. The central
 551 assumption of 10% intensification is highlighted with a cyan-colored median in the box plots.
 552 The second quartile Q2 (median) of the box plot is shown in orange/cyan, whiskers are placed
 553 at $\pm 1.5 \cdot$ interquartile range (Q3-Q1).

544 4 Discussion and conclusions

555 With more than one degree of global warming, most, if not all, extreme weather events now
 556 can be assumed to bear some imprint of climate change. By extension, this is also true for the
 557 humanitarian crises induced by catastrophic storms, floods, or droughts. However, while
 558 economic damages from climate change have been attributed both in case studies and global

560 studies (Frame et al., 2020b, 2020a; Sauer et al., 2021; Strauss et al., 2021), little is known
561 about the extent to which climate change has already exacerbated human displacement. Our
562 modeling study of TC Idai suggests that climate change may have induced between 12,600
563 (2.7%; lowest estimate under the no tide assumption) and 14,900 (3.2%; highest estimate
564 under the maximum tide assumption) additional displacements from this one event. This is
565 primarily due to the intensification of TC wind speed inducing a more powerful storm surge;
566 and to a lesser extent due to sea level rise providing a higher baseline for the storm surge.
567 We also show that the sensitivity of the results to the choice of TC intensification is
568 approximately in the same range as for the tide assumption. We note that our attribution
569 statements are, as commonly in the climate (impacts) attribution literature, purely statistical;
570 that is, we do not make any claims about whether or to what extent any individual person may
571 have been displaced because of climate change. Our methodology and results are subject to
572 a variety of limitations and uncertainties, primarily related to the models (coastal, fluvial, DEM)
573 and underlying datasets (population, displacement). Additional sources of uncertainty are the
574 counterfactual input quantities (SLR, wind speed intensification), impact flood levels, and tide
575 assumption, for which we perform sensitivity analyses.

577 Our results likely underestimate the full contribution of climate change to displacement
578 associated with TC Idai, because we solely addressed the effect of climate change on coastal
579 flooding, neglecting changes in inland flooding. Between March 3 and 17, heavy precipitation
580 between 200-400 mm was registered for Beira City and the region, with upstream sections of
581 the Pungwe River basin exposed to more than 600 mm (Probst and Annunziato, 2019). With
582 growing evidence that climate change not only affects precipitation intensity (Fowler et al.,
583 2021; Guerreiro et al., 2018; Scherrer et al., 2016) but also continental-scale changes in fluvial
584 flood discharge (Blöschl et al., 2019; Gudmundsson et al., 2021), it is likely that in a world
585 without climate change, the river flood magnitude would have been smaller, and even less
586 people would have been exposed than in our coastal-only counterfactual. Quantifying this
587 additional effect would require a river flood model capable of reproducing the observed flood
588 extent and associated inundation depths, and ideally, coupled with a coastal flood model to
589 capture the interaction between river flood and storm surge. Even though globally-applicable
590 frameworks for compound flood hazard modeling are under construction, and have recently
591 been tested for TC Idai (Eilander et al., 2022), evaluations of fluvial flood models reveal
592 important shortcomings in data-scarce regions such as Mozambique (Bernhofen et al., 2018;
593 Mester et al., 2021). Quantifying the role of river flooding in TC-induced displacement thus is
594 a timely challenge.

596 The inland river flood estimates based on satellite imagery exhibit several limitations and
597 uncertainties. In the absence of validation data, it is difficult to quantify the uncertainty arising
598 from the inland flood depths estimation. These gridded values are highly sensitive to the input
599 layers, namely the DEM (MERIT), permanent surface water (JRC), and the satellite-based
600 observation of inundation extents (FloodScan) (Atmospheric and Environmental Research &
601 African Risk Capacity, 2022). Especially uncertainties regarding the choice of DEM, used for
602 both the inland flood depth estimation and the coastal flood model, should not be neglected
603 (Hawker et al., 2018). Qualitatively, the performance seems poor in areas with higher
604 elevations (>20m). This could be attributable to challenges in representing the topography at
605 90 m resolution and dense obstructions that scatter returning signals (Shen et al., 2019).

606

Deleted:

608 Similarly, no suitable validation data for the coastal flood simulations is available. According to the [FloodScan](#) description (Atmospheric and Environmental Research & African Risk Capacity, 2022), the used products “depict large scale, inland river flooding well but are less likely to depict flooding in smaller floodplains and near coastlines”. We have hence opted to not choose the [FloodScan](#) product as the sole coastal flood hazard estimate nor as validation dataset for the flood extent from our coastal flood model. A flood risk screening for Beira (van Berchum et al., 2020) showed that simulated flood extent for a 10-year rainfall event plus a 10-year coastal surge event covers most parts of the Central and Munhava city districts of Beira (South-Eastern city districts). In contrast, the [FloodScan](#) product shows only little flooding in this area, while it is assumed that flooding by TC Idai exceeded an average recurrence interval of 10 years. For example, Emerton et al. (2020) show that GloFAS flood forecasts indicated a 100% probability of exceeding the severe flood alert threshold (20-year return period) for TC Idai at the Pungwe River (Emerton et al., 2020). Furthermore, newspaper photographs (Bergensia, 2019) show flooding in the Area de Baixa part of Beira (Western district of Beira), which was only partially flooded according to the satellite imagery. The AER product thus likely underestimates flood extent, which may be explained by cloud obscurement or failure in automatic flood detection due to, for example, flooding in densely populated areas, or the satellite passing over some time after the peak flooding when water levels have already receded.

627 Furthermore, the coastal flood modeling framework does not incorporate any astronomical tidal dynamics. Because there are no tide gauge records available in the region, we were only able to compare the model’s surge heights to the state-of-the-art Global Tide and Surge Model (GTSM). For the derived flood maps, there were no observational benchmarks available for validation. Moreover, the model is not able to take the interaction of the coastal surge with increased river discharge at the estuaries into account. In some cases, this interaction has been shown to influence water levels in a nonlinear way, for example for the 2016 Louisiana flood (Bilskie and Hagen, 2018). Another source of uncertainty is again the DEM, in particular the transition from topographic to bathymetric data at the coast lines.

637 Additionally, our analysis may be sensitive to the choice of population dataset (Archila Bustos et al., 2020; Leyk et al., 2019), which may lead to uncertainties regarding our estimated exposure. [One of the main error sources for population datasets is related to the areal interpolation methods to disaggregate the population data \(Archila Bustos et al., 2020\). GHS-POP distributes population only within built-up areas, which has the downside that non-residential areas are simulated as populated as well \(Freire et al., 2016\). In fact, a comparison with satellite imagery reveals that some areas in Beira are populated which are most likely only commercial or industrial sites. On the other hand, not all settlements are captured by GHS-POP, most likely due to their building type. Nonetheless, GHS-POP is still one of most accurate datasets in estimating and modeling the known population \(Archila Bustos et al., 2020\), especially in urban contexts \(Leyk et al., 2019\) as in the case for Beira.](#)

650 No information is available regarding the spatial distribution of displacements within GIDD; we assume that vulnerability to displacement is uniform across the affected area. The total number of displacements is furthermore not specifically categorized by hazard type, which reflects the multivariate (wind, rain and flood) compound characteristic of TCs hazards (Zscheischler et al., 2020). However, this impedes the attribution of coastal flood-induced displacements. Furthermore, the GIDD estimates include different forms of displacement,

Deleted: AER

Deleted: AER

Deleted: satellite imagery by

Deleted: AER

660 such as forced displacement or pre-emptive evacuations, with the latter potentially accounting
661 for a substantial proportion (McAdam, 2022). This poses far-reaching implications for
662 displacement risk modeling, as evacuations may already be triggered by lower flood depths,
663 or by early warnings of an impending hazard, which may not materialize in the expected
664 manner, or may not cause the level of destruction that would lead to a corresponding
665 magnitude of forced displacement.

666
667 Our main analysis also assumed no direct effect of high wind speeds on displacement, lacking
668 clear evidence for substantial displacement due to high winds alone. Our additional sensitivity
669 analysis suggests that changing this assumption could increase the number of displacements
670 attributable to climate change considerably. Given this potentially large effect, and our limited
671 understanding of the relative roles of different drivers of displacement in general, the specific
672 vulnerability to displacement from different types of hazard should be the subject of future
673 studies. Moreover, assuming that displacement can occur already at inundation depths of less
674 than 100 cm also leads to higher estimates of climate change-attributable displacement,
675 according to our sensitivity analysis. We also tested if the flood_{depth} threshold can be
676 estimated from the data by summing up the affected people per 10 cm flood depth increment
677 until equaling the number of observed displacements. This analysis yields an alternative flood_{depth}
678 threshold of 400 cm, which we assess to be physically not reasonable in the context of
679 building structure in Mozambique. Again, a better understanding of vulnerability beyond hard
680 physical flood_{depth} thresholds and empirically derived vulnerability factors will be critical to
681 refine risk assessments. Future work may produce a functional relationship between
682 displacement risk, contextual drivers, and physical flood properties, covering, for example,
683 depth, velocity, and duration.

684
685 We did not change storm track or size in our counterfactual simulations. While storm tracks
686 may be affected by climate change (Knutson et al., 2019), we assume that Beira has not
687 become more or less likely as a landfall site. Mean storm size is found to increase
688 systematically with the relative sea surface temperature (Chavas et al., 2016), although
689 numerical simulations suggest that projected median sizes remain nearly constant globally
690 (Knutson et al., 2015). Assuming increases in storm size due to climate change would again
691 result in higher estimates of attributable displacements in our analysis. By design, in our
692 attribution study, we assumed a fixed population distribution in both factual and counterfactual
693 simulations, as well as a fixed, empirically determined displacement vulnerability factor, and
694 only investigated changes in displacement risk following from changes in the physical
695 characteristics of TC Idai and its impacts. Assessments of future risks - or of past impacts -
696 should not only take into account the intensification of physical hazards, but also changes in
697 exposure (Kam et al., 2021); as well as potential changes in vulnerability due to social,
698 economic, or technological developments. For instance, TC-related displacements depend not
699 only on the damage to housing, but also on other factors such as government responsiveness
700 or poverty levels (Cissé et al., 2022). Here, we have chosen a storyline approach for the impact
701 attribution instead of a more traditional probabilistic attribution approach (Philip et al., 2020;
702 Titley et al., 2016), as for instance previously employed to attribute heavy precipitation of
703 Hurricane Harvey (Oldenborgh et al., 2017) to climate change. One reason is that for
704 Mozambique neither the complete time series of rainfall nor the high station density required
705 by a probabilistic approach (van Oldenborgh et al., 2021) are available. Reanalysis products
706 for precipitation could be used as an alternative, however, their quality depends on geographic
707 location, so the use of multiple reanalysis and/or observation products is recommended

Deleted:

Deleted:

Deleted:

Deleted: ¶

Deleted: ¶

Deleted: ¶

714 (Angéllil et al., 2016). Nonetheless, a climate attribution approach focusing on changes in the
715 probability or intensity of TCs in the South Indian Ocean due to anthropogenic forcing (O'Neill
716 et al., 2022) could guide the construction of counterfactual scenarios of the storyline approach.
717 Further, in contrast to the probabilistic approach, the storyline approach allows us to
718 investigate the driving factors involved, as well as their plausibility (Shepherd et al., 2018).
719

720 Framing the risk of tropical cyclones in the context of climate change in an event-specific rather
721 than a probabilistic manner also allows us to assign absolute numbers of attributable
722 displacements, which raises risk awareness in a more tangible way. Even though these
723 numbers include substantial and important uncertainties related to the models, datasets and
724 counterfactual assumptions, as discussed above, they provide an informative quantitative
725 indication of the additional risk posed by climate change to communities affected by one of
726 the worst natural disasters in recent history. The responsibility for managing and reducing
727 displacement risk lies primarily at the national and provincial level, but often local authorities,
728 organizations, and communities respond to displacement disasters (Hollinger and
729 Sienkevych, 2019). Demonstrating quantitatively how climate change affects the societal risks
730 associated with natural hazards may play an important role in raising awareness, with different
731 types of stakeholders, to the changing nature of such risks. It may also incentivize
732 governments to step up their efforts both in terms of planning and investing into adaptation
733 measures, and rapidly mitigating greenhouse gas emissions. The storyline approach is
734 particularly suited for highlighting the risk-amplifying effects of climate change in a tangible
735 and accessible way, based on a well-known event in the recent past (van den Hurk et al.,
736 2023). Estimates of the costs of displacement additionally highlight the adverse economic
737 aspects of climate change (Desai et al., 2021); average costs have been put at \$310 per
738 displaced person per year, though actual costs are heavily dependent on the country and
739 duration (days/weeks to years) (IDMC, 2019). Only 50.7% of the required Mozambique
740 Humanitarian Response Plan 2019 of US\$m 620.5 was funded, demonstrating that climate
741 change poses an additional burden to insufficiently equipped financial aid resources.
742 Anticipating the intensification of tropical cyclones under future global warming (Knutson et
743 al., 2020) calls for enhancing adaptation measures as well as disaster relief and humanitarian
744 aid. The IPCC AR6 projects an additional global increase in mean sea level and surface
745 temperature of 0.44 m / 1.2°C (SSP1-2.6) and 0.77 m / 4.0°C (SSP5-8.5), relative to a baseline
746 of 1995-2014, by the end of the 21st century (Fox-Kemper et al., 2021; Lee et al., 2021). Even
747 though these increases may vary between basins, an enhanced displacement risk due to Idai-
748 like TCs needs to be accounted for in the next decades, especially if future changes in
749 exposure due to population growth and urbanization are considered. Under both SSPs 1 and
750 5, the population of Mozambique is projected to increase by approximately 8 million, and its
751 urbanization level from about 40% to over 70%, just over the next 30 years (Riahi et al., 2017).
752

753 Our study expands the scope of extreme event impact attribution to include displacement as
754 a societal impact dimension. In general, due to the lack of calibrated regional models and
755 gauge stations, only few attribution studies (Luu et al., 2021; Takayabu et al., 2015) focus on
756 storms - or any extreme weather events, for that matter - in low-income countries. This not
757 only limits our understanding of climate change effects on extreme events from a global
758 perspective, but also biases geographically the amount of knowledge and information
759 available to inform risk management and adaptation strategies (Otto et al., 2020). Our impact
760 attribution is built on global-scale datasets and models, which could be employed in other
761 relevant locations. Despite the discussed limitations and uncertainties inherent to this

762 approach, displacements could be similarly attributed to climate change for other major TCs
763 that occurred in data- and model-scarce regions, such as Typhoon Haiyan (Philippines; 4.1
764 million displacements) or Cyclone Amphan (India and Bangladesh; combined 4.95 million
765 displacements) (IDMC, 2022). The continuing increase in spatial resolution of global-scale
766 products will eventually allow for more granular displacement risk assessments, which
767 regional authorities could incorporate in urban development plans, zoning regulations or
768 required building codes (IDMC, 2019). Mozambique, like many countries, is exposed not only
769 to TCs but also other climate-related hazards, such as droughts, and at the same time facing
770 socio-economic challenges, making it all the more important to understand and anticipate risks
771 in a changing climate. Our approach may hence be extended to large-n impact attribution,
772 using, for example, global counterfactual climate datasets (Mengel et al., 2021).

Deleted:

773 Code availability

774 The source code for this study is available from
775 https://github.com/BenediktMester/TC_Idai_attriubution.
776

777 Data availability

778 Satellite imagery is used with the permission of Atmospheric and Environmental Research &
779 African Risk Capacity. Output of the flood depth algorithm, GeoClaw results, and TC Idai wind
780 speed files can be accessed at <https://zenodo.org/record/6907855> (Mester et al., 2022). GHS
781 gridded population data is available at https://data.jrc.ec.europa.eu/dataset/jrc-ghsl-ghs_pop_gpww4_globe_r2015a#dataaccess.

782 National borders of Mozambique were obtained from <https://qadm.org/data.html>. For the
783 trendline analysis of annual means of maximum wind speeds we use IBTrACS Version 4
784 database, accessible at <https://www.ncei.noaa.gov/data/international-best-track-archive-for-climate-stewardship-ibtracs/v04r00/access/netcdf/IBTrACS.ALL.v04r00.nc>.

785
786
787 All data used for the figures are publicly available. Maps were generated with QGIS, which
788 can be downloaded at <https://www.qgis.org/>. Satellite imagery background by © Google Maps
789 can be accessed via <http://mt0.google.com/vt/lyrs=s&hl=en&x={x}&y={y}&z={z}>. We used
790 IBTrACS Version 4 to extract the trajectory data of tropical cyclone Idai, available at
791 <https://www.ncei.noaa.gov/products/international-best-track-archive?name=ib-v4-access>.

792 Mozambique admin level 4 shapefiles for Beira are available at
793 <https://data.humdata.org/dataset/mozambique-admin-level-4-beira-and-dondo->
794 [neighbourhood-boundaries](https://data.humdata.org/dataset/mozambique-admin-level-4-beira-and-dondo-). GSHHG shoreline data can be accessed via
795 <https://www.ngdc.noaa.gov/mgg/shorelines/data/qshhg/latest/>.
796

797 Author contributions

798 B.M. and J.S. designed the study, with contributions from T.V., C.O., and K.F. T.V. designed
799 and performed coastal flood model calculations. S.B. estimated flood depths from satellite
800 imagery. B.M. computed the number of affected people and displacements. B.M. and J.S.

802 analyzed the results, and C.O. and K.F. contributed to the interpretation. B.M. and J.S. jointly
803 wrote the paper, with contributions from T.V., S.B., and C.O.

804 Competing interests

805 The authors declare no competing interests.

806 Acknowledgments

807 This research received funding from the European Union's Horizon 2020 research and
808 innovation programme under grant agreement No 820712 (RECEIPT). [T.V. received funding](#)
809 [from the German Federal Ministry of Education and Research \(BMBF\) under the research](#)
810 [project QUIDIC \(01LP1907A\), and through the CHIPS project, part of AXIS, an ERA-NET](#)
811 [initiated by JPI Climate, and funded by FORMAS \(SE\), DLR/BMBF \(DE, Grant No.](#)
812 [01LS1904A\), AEI \(ES\) and ANR \(FR\) with co-funding by the European Union \(Grant No.](#)
813 [776608\).](#)

814

815 References

816

- 817 Angéil, O., Perkins-Kirkpatrick, S., Alexander, L.V., Stone, D., Donat, M.G., Wehner, M.,
818 Shiogama, H., Ciavarella, A., Christidis, N., 2016. Comparing regional precipitation
819 and temperature extremes in climate model and reanalysis products. *Weather Clim.*
820 *Extrem.* 13, 35–43. <https://doi.org/10.1016/j.wace.2016.07.001>
- 821 Archila Bustos, M.F., Hall, O., Niedomysl, T., Ernstson, U., 2020. A pixel level evaluation of
822 five multitemporal global gridded population datasets: a case study in Sweden,
823 1990–2015. *Popul. Environ.* 42, 255–277. [https://doi.org/10.1007/s11111-020-00360-](https://doi.org/10.1007/s11111-020-00360-8)
824 [8](https://doi.org/10.1007/s11111-020-00360-8)
- 825 Atmospheric and Environmental Research & African Risk Capacity, 2022. Flood depictions:
826 AER AFED v05r01.
- 827 Beal, L.M., Vialard, J., Roxy, M.K., lead authors, 2019. IndOOS-2: A roadmap to sustained
828 observations of the Indian Ocean for 2020-203 CLIVAR-4/2019, GOOS-237, 206 pp.,
829 218.
- 830 Bergensia, 2019. Red Cross: 90 Percent of Beira in Mozambique Destroyed by Cyclone Idai.
831 URL: [https://bergensia.com/red-cross-90-percent-of-beira-in-mozambique-destroyed-](https://bergensia.com/red-cross-90-percent-of-beira-in-mozambique-destroyed-by-cyclone-idai/)
832 [by-cyclone-idai/](https://bergensia.com/red-cross-90-percent-of-beira-in-mozambique-destroyed-by-cyclone-idai/).
- 833 Bernhofen, M.V., Whyman, C., Trigg, M.A., Sleigh, P.A., Smith, A.M., Sampson, C.C.,
834 Yamazaki, D., Ward, P.J., Rudari, R., Pappenberger, F., Dottori, F., Salamon, P.,
835 Winsemius, H.C., 2018. A first collective validation of global fluvial flood models for
836 major floods in Nigeria and Mozambique. *Environ. Res. Lett.* 13, 104007.
837 <https://doi.org/10.1088/1748-9326/aae014>
- 838 Bilskie, M.V., Hagen, S.C., 2018. Defining Flood Zone Transitions in Low-Gradient Coastal
839 Regions. *Geophys. Res. Lett.* 45, 2761–2770. <https://doi.org/10.1002/2018GL077524>
- 840 Bloemendaal, N., de Moel, H., Martinez, A.B., Muis, S., Haigh, I.D., van der Wiel, K.,
841 Haarsma, R.J., Ward, P.J., Roberts, M.J., Dullaart, J.C.M., Aerts, J.C.J.H., 2022. A
842 globally consistent local-scale assessment of future tropical cyclone risk. *Sci. Adv.* 8,
843 eabm8438. <https://doi.org/10.1126/sciadv.abm8438>

- 844 Bloemendaal, N., Haigh, I.D., de Moel, H., Muis, S., Haarsma, R.J., Aerts, J.C.J.H., 2020.
845 Generation of a global synthetic tropical cyclone hazard dataset using STORM. *Sci.*
846 *Data* 7, 40. <https://doi.org/10.1038/s41597-020-0381-2>
- 847 Bloemendaal, N., Moel, H. de, Mol, J.M., Bosma, P.R.M., Polen, A.N., Collins, J.M., 2021.
848 Adequately reflecting the severity of tropical cyclones using the new Tropical Cyclone
849 Severity Scale. *Environ. Res. Lett.* 16, 014048. <https://doi.org/10.1088/1748-9326/abd131>
- 850 Blöschl, G., Hall, J., Viglione, A., Perdigão, R.A.P., Parajka, J., Merz, B., Lun, D., Arheimer,
851 B., Aronica, G.T., Bilibashi, A., Boháč, M., Bonacci, O., Borga, M., Čanjevac, I.,
852 Castellarin, A., Chirico, G.B., Claps, P., Frolova, N., Ganora, D., Gorbachova, L., Gül,
853 A., Hannaford, J., Harrigan, S., Kireeva, M., Kiss, A., Kjeldsen, T.R., Kohnová, S.,
854 Koskela, J.J., Ledvinka, O., Macdonald, N., Mavrova-Guirguinova, M., Mediero, L.,
855 Merz, R., Molnar, P., Montanari, A., Murphy, C., Osuch, M., Ovcharuk, V., Radevski,
856 I., Salinas, J.L., Sauquet, E., Šraj, M., Szolgay, J., Volpi, E., Wilson, D., Zaimi, K.,
857 Živković, N., 2019. Changing climate both increases and decreases European river
858 floods. *Nature* 573, 108–111. <https://doi.org/10.1038/s41586-019-1495-6>
- 859 Bryant, S., McGrath, H., Boudreault, M., 2022. Gridded flood depth estimates from satellite-
860 derived inundations. *Nat. Hazards Earth Syst. Sci.* 22, 1437–1450.
861 <https://doi.org/10.5194/nhess-22-1437-2022>
- 862 Cattaneo, C., Beine, M., Fröhlich, C.J., Kniveton, D., Martinez-Zarzoso, I., Mastrotrillo, M.,
863 Millock, K., Pigué, E., Schraven, B., 2019. Human Migration in the Era of Climate
864 Change. *Rev. Environ. Econ. Policy* 13, 189–206.
865 <https://doi.org/10.1093/reep/rez008>
- 866 Chavas, D.R., Lin, N., Dong, W., Lin, Y., 2016. Observed Tropical Cyclone Size Revisited. *J.*
867 *Clim.* 29, 2923–2939. <https://doi.org/10.1175/JCLI-D-15-0731.1>
- 868 Church, J.A., Clark, P.U., Cazenave, A., Gregory, J.M., Jevrejeva, S., Levermann, A.,
869 Merrifield, M.A., Milne, G.A., Nerem, R.S., Nunn, P.D., Payne, A.J., Pfeffer, W.T.,
870 Stammer, D., Unnikrishnan, A.S., 2013. Sea Level Change. In: *Climate Change*
871 *2013: The Physical Science Basis. Contribution of Working Group I to the Fifth*
872 *Assessment Report of the Intergovernmental Panel on Climate Change* [Stocker,
873 T.F., D. Qin, G.-K. Plattner, M. Tignor, S.K. Allen, J. Boschung, A. Nauels, Y. Xia, V.
874 Bex and P.M. Midgley (eds.)]. Cambridge University Press, Cambridge, United
875 Kingdom and New York, NY, USA, pp. 1137–1216.
- 876 Church, J.A., White, N.J., 2011. Sea-Level Rise from the Late 19th to the Early 21st Century.
877 *Surv. Geophys.* 32, 585–602. <https://doi.org/10.1007/s10712-011-9119-1>
- 878 Church, J.A., White, N.J., Coleman, R., Lambeck, K., Mitrovica, J.X., 2004. Estimates of the
879 Regional Distribution of Sea Level Rise over the 1950–2000 Period. *J. Clim.* 17,
880 2609–2625. [https://doi.org/10.1175/1520-0442\(2004\)017<2609:EOTRDO>2.0.CO;2](https://doi.org/10.1175/1520-0442(2004)017<2609:EOTRDO>2.0.CO;2)
- 881 Cissé, G., McLeman, R., Adams, H., Aldunce, P., Bowen, K., Campbell-Lendrum, D.,
882 Clayton, S., Ebi, K.L., Hess, J., Huang, C., Liu, Q., McGregor, G., Semenza, J.,
883 Tirado, M.C., 2022. Health, Wellbeing, and the Changing Structure of Communities.
884 In: *Climate Change 2022: Impacts, Adaptation, and Vulnerability. Contribution of*
885 *Working Group II to the Sixth Assessment Report of the Intergovernmental Panel on*
886 *Climate Change* [H.-O. Pörtner, D.C. Roberts, M. Tignor, E.S. Poloczanska, K.
887 Mintenbeck, A. Alegría, M. Craig, S. Langsdorf, S. Lösche, V. Möller, A. Okem, B.
888 Rama (eds.)]. Cambridge University Press, Cambridge, UK and New York, NY, USA,
889 pp. 1041-1170, doi:10.1017/9781009325844.009.
- 890 CMEMS, 2021. Global ocean gridded L4 sea surface heights and derived variables
891 reprocessed (1993-ongoing). E.U. Copernicus Marine Service (CMEMS).
892 Downloaded 2021-08-02.
- 893 Cohen, S., Brakenridge, G.R., Kettner, A., Bates, B., Nelson, J., McDonald, R., Huang, Y.-F.,
894 Munasinghe, D., Zhang, J., 2018. Estimating Floodwater Depths from Flood
895 Inundation Maps and Topography. *JAWRA J. Am. Water Resour. Assoc.* 54, 847–
896 858. <https://doi.org/10.1111/1752-1688.12609>
- 897 Custer, R., Nishijima, K., 2015. Flood vulnerability assessment of residential buildings by

899 explicit damage process modelling. *Nat. Hazards* 78, 461–496.
900 <https://doi.org/10.1007/s11069-015-1725-7>

901 Dangendorf Sönke, Marcos Marta, Wöppelmann Guy, Conrad Clinton P., Frederikse
902 Thomas, Riva Riccardo, 2017. Reassessment of 20th century global mean sea level
903 rise. *Proc. Natl. Acad. Sci.* 114, 5946–5951.
904 <https://doi.org/10.1073/pnas.1616007114>

905 Desai, B., Bresch, D.N., Cazabat, C., Hochrainer-Stigler, S., Mechler, R., Ponserre, S.,
906 Schewe, J., 2021. Addressing the human cost in a changing climate. *Science* 372,
907 1284–1287. <https://doi.org/10.1126/science.abh4283>

908 Dullaart, J.C.M., Muis, S., Bloemendaal, N., Chertova, M.V., Couasnon, A., Aerts, J.C.J.H.,
909 2021. Accounting for tropical cyclones more than doubles the global population
910 exposed to low-probability coastal flooding. *Commun. Earth Environ.* 2, 135.
911 <https://doi.org/10.1038/s43247-021-00204-9>

912 Eilander, D., Couasnon, A., Leijnse, T., Ikeuchi, H., Yamazaki, D., Muis, S., Dullaart, J.,
913 Winsemius, H.C., Ward, P.J., 2022. A globally-applicable framework for compound
914 flood hazard modeling. *EGU sphere* 2022, 1–40. [https://doi.org/10.5194/egusphere-](https://doi.org/10.5194/egusphere-2022-149)
915 [2022-149](https://doi.org/10.5194/egusphere-2022-149)

916 Emanuel, K., 2005. Increasing destructiveness of tropical cyclones over the past 30 years.
917 *Nature* 436, 686–688. <https://doi.org/10.1038/nature03906>

918 Emanuel, K., Ravela, S., Vivant, E., Risi, C., 2006. A Statistical Deterministic Approach to
919 Hurricane Risk Assessment. *Bull. Am. Meteorol. Soc.* 87, 299–314.
920 <https://doi.org/10.1175/BAMS-87-3-299>

921 Emanuel, K.A., 2013. Downscaling CMIP5 climate models shows increased tropical cyclone
922 activity over the 21st century. *Proc. Natl. Acad. Sci. U. S. A.* 110, 12219–12224.
923 <https://doi.org/10.1073/pnas.1301293110>

924 Emanuel, K.A., 1987. The dependence of hurricane intensity on climate. *Nature* 326, 483–
925 485. <https://doi.org/10.1038/326483a0>

926 Emerton, R., Cloke, H., Ficchi, A., Hawker, L., de Wit, S., Speight, L., Prudhomme, C.,
927 Rundell, P., West, R., Neal, J., Cuna, J., Harrigan, S., Titley, H., Magnusson, L.,
928 Pappenberger, F., Klingaman, N., Stephens, E., 2020. Emergency flood bulletins for
929 Cyclones Idai and Kenneth: A critical evaluation of the use of global flood forecasts
930 for international humanitarian preparedness and response. *Int. J. Disaster Risk*
931 *Reduct.* 50, 101811. <https://doi.org/10.1016/j.ijdrr.2020.101811>

932 Fowler, H.J., Lenderink, G., Prein, A.F., Westra, S., Allan, R.P., Ban, N., Barbero, R., Berg,
933 P., Blenkinsop, S., Do, H.X., Guerreiro, S., Haerter, J.O., Kendon, E.J., Lewis, E.,
934 Schaer, C., Sharma, A., Villarini, G., Wasko, C., Zhang, X., 2021. Anthropogenic
935 intensification of short-duration rainfall extremes. *Nat. Rev. Earth Environ.* 2, 107–
936 122. <https://doi.org/10.1038/s43017-020-00128-6>

937 Fox-Kemper, B., Hewitt, H.T., Xiao, C., Aðalgeirsdóttir, G., Drijfhout, S.S., Edwards, T.L.,
938 Golledge, N.R., Hemer, M., Kopp, R.E., Krinner, G., Mix, A., Notz, D., Nowicki, S.,
939 Nurhati, I.S., Ruiz, L., Sallée, J.-B., Slangen, A.B.A., Yu, Y., 2021. Ocean,
940 Cryosphere and Sea Level Change. In *Climate Change 2021: The Physical Science*
941 *Basis. Contribution of Working Group I to the Sixth Assessment Report of the*
942 *Intergovernmental Panel on Climate Change* [Masson-Delmotte, V., P. Zhai, A.
943 Pirani, S.L. Connors, C. Péan, S. Berger, N. Caud, Y. Chen, L. Goldfarb, M.I. Gomis,
944 M. Huang, K. Leitzell, E. Lonnoy, J.B.R. Matthews, T.K. Maycock, T. Waterfield, O.
945 Yelekçi, R. Yu, and B. Zhou (eds.)]. Cambridge University Press, Cambridge, United
946 Kingdom and New York, NY, USA, pp. 1211–1362.

947 Frame, D.J., Rosier, S.M., Noy, I., Harrington, L.J., Carey-Smith, T., Sparrow, S.N., Stone,
948 D.A., Dean, S.M., 2020a. Climate change attribution and the economic costs of
949 extreme weather events: a study on damages from extreme rainfall and drought.
950 *Clim. Change* 162, 781–797. <https://doi.org/10.1007/s10584-020-02729-y>

951 Frame, D.J., Wehner, M.F., Noy, I., Rosier, S.M., 2020b. The economic costs of Hurricane
952 Harvey attributable to climate change. *Clim. Change* 160, 271–281.
953 <https://doi.org/10.1007/s10584-020-02692-8>

954 Freire, S., MacManus, K., Pesaresi, M., Doxsey-Whitfield, E., Mills, J., 2016. Development of
955 new open and free multi-temporal global population grids at 250m resolution. Paper
956 presented at the 19th AGILE Conference on Geographic Information Science,
957 Helsinki, Finland.

958 GADM, 2018. Database of Global Administrative Areas.

959 Galantowicz, J.F., Picton, J., 2021. Flood Mapping with Passive Microwave Remote
960 Sensing: Current Capabilities and Directions for Future Development, in: *Earth
961 Observation for Flood Applications*. Elsevier, p. 28.

962 Garner Andra J., Mann Michael E., Emanuel Kerry A., Kopp Robert E., Lin Ning, Alley
963 Richard B., Horton Benjamin P., DeConto Robert M., Donnelly Jeffrey P., Pollard
964 David, 2017. Impact of climate change on New York City's coastal flood hazard:
965 Increasing flood heights from the preindustrial to 2300 CE. *Proc. Natl. Acad. Sci.* 114,
966 11861–11866. <https://doi.org/10.1073/pnas.1703568114>

967 Geiger, T., Frieler, K., Bresch, D.N., 2018. A global historical data set of tropical cyclone
968 exposure (TCE-DAT). *Earth Syst. Sci. Data* 10, 185–194.
969 <https://doi.org/10.5194/essd-10-185-2018>

970 Gemenne, F., 2011. Why the numbers don't add up: A review of estimates and predictions of
971 people displaced by environmental changes. *Glob. Environ. Change, Migration and
972 Global Environmental Change – Review of Drivers of Migration* 21, S41–S49.
973 <https://doi.org/10.1016/j.gloenvcha.2011.09.005>

974 Google Maps (a), 2022. Mozambique. Satellite image. URL:
975 <http://mt0.google.com/vt/lyrs=s&hl=en&x={x}&y={y}&z={z}>. Accessed on 2022-04-27.

976 Google Maps (b), 2022. Greater Area of Beira, Mozambique. Satellite image. URL:
977 <http://mt0.google.com/vt/lyrs=s&hl=en&x={x}&y={y}&z={z}>. Accessed on 2022-04-27.

978 Gudmundsson, L., Boulange, J., Do, H.X., Gosling, S.N., Grillakis, M.G., Koutroulis, A.G.,
979 Leonard, M., Liu, J., Müller Schmied, H., Papadimitriou, L., Pokhrel, Y., Seneviratne,
980 S.I., Satoh, Y., Thiery, W., Westra, S., Zhang, X., Zhao, F., 2021. Globally observed
981 trends in mean and extreme river flow attributed to climate change. *Science* 371,
982 1159–1162. <https://doi.org/10.1126/science.aba3996>

983 Guerreiro, S.B., Fowler, H.J., Barbero, R., Westra, S., Lenderink, G., Blenkinsop, S., Lewis,
984 E., Li, X.-F., 2018. Detection of continental-scale intensification of hourly rainfall
985 extremes. *Nat. Clim. Change* 8, 803–807. <https://doi.org/10.1038/s41558-018-0245-3>

986 Guha-Sapir, D., Below, R., Hoyois, P., 2022. EM-DAT: The CRED/OFDA International
987 Disaster Database. Université Catholique de Louvain-Brussels, Belgium.

988 Gulev, S.K., Thorne, P.W., Ahn, J., Dentener, F.J., Domingues, C.M., Gerland, S., Gong, D.,
989 Kaufman, D.S., Nnamchi, H.C., Quaas, J., Rivera, J.A., Sathyendranath, S., Smith,
990 S.L., Trewin, B., von Schuckmann, K., Vose, R.S., 2021. Changing State of the
991 Climate System. In *Climate Change 2021: The Physical Science Basis. Contribution
992 of Working Group I to the Sixth Assessment Report of the Intergovernmental Panel
993 on Climate Change* [Masson-Delmotte, V., P. Zhai, A. Pirani, S.L. Connors, C. Péan,
994 S. Berger, N. Caud, Y. Chen, L. Goldfarb, M.I. Gomis, M. Huang, K. Leitzell, E.
995 Lonnoy, J.B.R. Matthews, T.K. Maycock, T. Waterfield, O. Yelekçi, R. Yu, and B.
996 Zhou (eds.)]. Cambridge University Press. In Press.

997 Han, W., Meehl, G.A., Rajagopalan, B., Fasullo, J.T., Hu, A., Lin, J., Large, W.G., Wang, J.,
998 Quan, X.-W., Trenary, L.L., Wallcraft, A., Shinoda, T., Yeager, S., 2010. Patterns of
999 Indian Ocean sea-level change in a warming climate. *Nat. Geosci.* 3, 546–550.
1000 <https://doi.org/10.1038/ngeo901>

1001 HDX, 2019. Mozambique admin level 4 - Beira and Dondo neighbourhood boundaries.

1002 Holland, G.J., 1980. An Analytic Model of the Wind and Pressure Profiles in Hurricanes.
1003 *Mon. Weather Rev.* 108, 1212–1218. [https://doi.org/10.1175/1520-0493\(1980\)108<1212:AAMOTW>2.0.CO;2](https://doi.org/10.1175/1520-0493(1980)108<1212:AAMOTW>2.0.CO;2)

1004 Hollinger, M., Sienkevych, O., 2019. The role of local and regional governments in protecting
1005 internally displaced persons (IDPs).

1006 IDMC, 2022. "IDMC Global Report on Internal Displacement 2022 Displacement Dataset."
1007 <https://www.internal-displacement.org/database/displacement-data>.

1009 IDMC, 2019. Unveiling the cost of internal displacement, The ripple effect: economic impacts
1010 of internal displacement.

1011 Irish, J.L., Sleath, A., Cialone, M.A., Knutson, T.R., Jensen, R.E., 2014. Simulations of
1012 Hurricane Katrina (2005) under sea level and climate conditions for 1900. *Clim.*
1013 *Change* 122, 635–649. <https://doi.org/10.1007/s10584-013-1011-1>

1014 Kam, P.M., Aznar-Siguan, G., Schewe, J., Milano, L., Ginnetti, J., Willner, S., McCaughey,
1015 J.W., Bresch, D.N., 2021. Global warming and population change both heighten
1016 future risk of human displacement due to river floods. *Environ. Res. Lett.* 16, 044026.
1017 <https://doi.org/10.1088/1748-9326/abd26c>

1018 Knapp, K.R., Kruk, M.C., Levinson, D.H., Diamond, H.J., Neumann, C.J., 2010. The
1019 International Best Track Archive for Climate Stewardship (IBTrACS): Unifying
1020 Tropical Cyclone Data. *Bulletin of the American Meteorological Society* 91 (3): 363-
1021 76.

1022 Knutson, T., Camargo, S.J., Chan, J.C.L., Emanuel, K., Ho, C.-H., Kossin, J., Mohapatra,
1023 M., Satoh, M., Sugi, M., Walsh, K., Wu, L., 2020. Tropical Cyclones and Climate
1024 Change Assessment: Part II: Projected Response to Anthropogenic Warming. *Bull.*
1025 *Am. Meteorol. Soc.* 101, E303–E322. <https://doi.org/10.1175/BAMS-D-18-0194.1>

1026 Knutson, T., Camargo, S.J., Chan, J.C.L., Emanuel, K., Ho, C.-H., Kossin, J., Mohapatra,
1027 M., Satoh, M., Sugi, M., Walsh, K., Wu, L., 2019. Tropical Cyclones and Climate
1028 Change Assessment: Part I: Detection and Attribution. *Bull. Am. Meteorol. Soc.* 100,
1029 1987–2007. <https://doi.org/10.1175/BAMS-D-18-0189.1>

1030 Knutson, T.R., Sirutis, J.J., Zhao, M., Tuleya, R.E., Bender, M., Vecchi, G.A., Villarini, G.,
1031 Chavas, D., 2015. Global Projections of Intense Tropical Cyclone Activity for the Late
1032 Twenty-First Century from Dynamical Downscaling of CMIP5/RCP4.5 Scenarios. *J.*
1033 *Clim.* 28, 7203–7224. <https://doi.org/10.1175/JCLI-D-15-0129.1>

1034 Kossin, J.P., Knapp, K.R., Vimont, D.J., Murnane, R.J., Harper, B.A., 2007. A globally
1035 consistent reanalysis of hurricane variability and trends. *Geophys. Res. Lett.* 34.
1036 <https://doi.org/10.1029/2006GL028836>

1037 Kossin, J.P., Olander, T.L., Knapp, K.R., 2013. Trend Analysis with a New Global Record of
1038 Tropical Cyclone Intensity. *J. Clim.* 26, 9960–9976. <https://doi.org/10.1175/JCLI-D-13-00262.1>

1040 Kulp, S.A., Strauss, B.H., 2021. CoastalDEM v2.1: A high-accuracy and high-resolution
1041 global coastal elevation model trained on ICESat-2 satellite lidar. *Climate Central*
1042 *Scientific Report* 17.

1043 Kulp, S.A., Strauss, B.H., 2018. CoastalDEM: A global coastal digital elevation model
1044 improved from SRTM using a neural network. *Remote Sens. Environ.* 206, 231–239.
1045 <https://doi.org/10.1016/j.rse.2017.12.026>

1046 Lee, J.-Y., Marotzke, J., Bala, G., Cao, L., Corti, S., Dunne, J.P., Engelbrecht, F., Fischer,
1047 E., Fyfe, J.C., Jones, C., Maycock, A., Mutemi, J., Ndiaye, O., Panickal, S., Zhou, T.,
1048 2021. Future Global Climate: Scenario-Based Projections and Near-Term
1049 Information. In *Climate Change 2021: The Physical Science Basis. Contribution of*
1050 *Working Group I to the Sixth Assessment Report of the Intergovernmental Panel on*
1051 *Climate Change* [Masson-Delmotte, V., P. Zhai, A. Pirani, S.L. Connors, C. Péan, S.
1052 Berger, N. Caud, Y. Chen, L. Goldfarb, M.I. Gomis, M. Huang, K. Leitzell, E. Lonnoy,
1053 J.B.R. Matthews, T.K. Maycock, T. Waterfield, O. Yelekçi, R. Yu, and B. Zhou (eds.)].
1054 C. Cambridge University Press, Cambridge, United Kingdom and New York, NY,
1055 USA, pp. 553–672.

1056 Leyk, S., Gaughan, A.E., Adamo, S.B., de Sherbinin, A., Balk, D., Freire, S., Rose, A.,
1057 Stevens, F.R., Blankespoor, B., Frye, C., Comenetz, J., Sorichetta, A., MacManus,
1058 K., Pistolesi, L., Levy, M., Tatem, A.J., Pesaresi, M., 2019. The spatial allocation of
1059 population: a review of large-scale gridded population data products and their fitness
1060 for use. *Earth Syst. Sci. Data* 11, 1385–1409. <https://doi.org/10.5194/essd-11-1385-2019>

1062 Lin, N., Emanuel, K., Oppenheimer, M., Vanmarcke, E., 2012. Physically based assessment
1063 of hurricane surge threat under climate change. *Nat. Clim. Change* 2, 462–467.

1064 <https://doi.org/10.1038/nclimate1389>
 1065 Lin, N., Lane, P., Emanuel, K.A., Sullivan, R.M., Donnelly, J.P., 2014. Heightened hurricane
 1066 surge risk in northwest Florida revealed from climatological-hydrodynamic modeling
 1067 and paleorecord reconstruction. *J. Geophys. Res. Atmospheres* 119, 8606–8623.
 1068 <https://doi.org/10.1002/2014JD021584>
 1069 Lindsay, J.B., 2014. The Whitebox Geospatial Analysis Tools Project and Open-Access GIS.
 1070 *Proc. GIS Res. UK 22nd Annu. Conf. Univ. Glasg.* 16–18.
 1071 Luu, L.N., Scussolini, P., Kew, S., Philip, S., Hariadi, M.H., Vautard, R., Van Mai, K., Van Vu,
 1072 T., Truong, K.B., Otto, F., van der Schrier, G., van Aalst, M.K., van Oldenborgh, G.J.,
 1073 2021. Attribution of typhoon-induced torrential precipitation in Central Vietnam,
 1074 October 2020. *Clim. Change* 169, 24. <https://doi.org/10.1007/s10584-021-03261-3>
 1075 Lyard, F.H., Allain, D.J., Cancet, M., Carrère, L., Picot, N., 2021. FES2014 global ocean tide
 1076 atlas: design and performance. *Ocean Sci.* 17, 615–649. <https://doi.org/10.5194/os-17-615-2021>
 1077
 1078 Mandli, K.T., Dawson, C.N., 2014. Adaptive mesh refinement for storm surge. *Ocean Model.*
 1079 75, 36–50. <https://doi.org/10.1016/j.ocemod.2014.01.002>
 1080 McAdam, J., 2022. Evacuations: a form of disaster displacement? *Forced Migr. Rev.* 56–57.
 1081 Mengel, M., Treu, S., Lange, S., Frieler, K., 2021. ATTRICI v1.1 – counterfactual climate for
 1082 impact attribution. *Geosci. Model Dev.* 14, 5269–5284. <https://doi.org/10.5194/gmd-14-5269-2021>
 1083
 1084 Mester, B., Vogt, T., Bryant, S., Otto, C., Frieler, K., Schewe, J., 2022. TC Idai attribution
 1085 study - data collection v1.1 (Version v1.1). doi: 10.5281/zenodo.6907855.
 1086 Mester, B., Willner, S.N., Frieler, K., Schewe, J., 2021. Evaluation of river flood extent
 1087 simulated with multiple global hydrological models and climate forcings. *Environ.*
 1088 *Res. Lett.* 16, 094010. <https://doi.org/10.1088/1748-9326/ac188d>
 1089 Muis, S., Apecechea, M.I., Dullaart, J., de Lima Rego, J., Madsen, K.S., Su, J., Yan, K.,
 1090 Verlaan, M., 2020. A High-Resolution Global Dataset of Extreme Sea Levels, Tides,
 1091 and Storm Surges, Including Future Projections. *Front. Mar. Sci.* 7.
 1092 <https://doi.org/10.3389/fmars.2020.00263>
 1093 Nicholls, R.J., Lincke, D., Hinkel, J., Brown, S., Vafeidis, A.T., Meyssignac, B., Hanson, S.E.,
 1094 Merkens, J.-L., Fang, J., 2021. A global analysis of subsidence, relative sea-level
 1095 change and coastal flood exposure. *Nat. Clim. Change* 11, 338–342.
 1096 <https://doi.org/10.1038/s41558-021-00993-z>
 1097 Nott, J., Hayne, M., 2001. High frequency of 'super-cyclones' along the Great Barrier Reef
 1098 over the past 5,000 years. *Nature* 413, 508–512. <https://doi.org/10.1038/35097055>
 1099 OCHA, 2004. Guiding Principles on Internal Displacement.
 1100 Oldenborgh, G.J. van, Wiel, K. van der, Sebastian, A., Singh, R., Arrighi, J., Otto, F.,
 1101 Haustein, K., Li, S., Vecchi, G., Cullen, H., 2017. Attribution of extreme rainfall from
 1102 Hurricane Harvey, August 2017. *Environ. Res. Lett.* 12, 124009.
 1103 <https://doi.org/10.1088/1748-9326/aa9ef2>
 1104 O'Neill, B., van Aalst, M., Zaiton Ibrahim, Z., Berrang Ford, L., Bhadwal, S., Buhaug, H.,
 1105 Diaz, D., Frieler, K., Garschagen, M., Magnan, A., Midgley, G., Mirzabaev, A.,
 1106 Thomas, A., Warren, R., 2022. Key Risks Across Sectors and Regions. In: *Climate*
 1107 *Change 2022: Impacts, Adaptation, and Vulnerability. Contribution of Working Group*
 1108 *II to the Sixth Assessment Report of the Intergovernmental Panel on Climate Change*
 1109 *[H.-O. Pörtner, D.C. Roberts, M. Tignor, E.S. Poloczanska, K. Mintenbeck, A.*
 1110 *Alegria, M. Craig, S. Langsdorf, S. Löschke, V. Möller, A. Okem, B. Rama (eds.)].*
 1111 Cambridge University Press.
 1112 Otto, F.E.L., Harrington, L., Schmitt, K., Philip, S., Kew, S., Oldenborgh, G.J. van, Singh, R.,
 1113 Kimutai, J., Wolski, P., 2020. Challenges to Understanding Extreme Weather
 1114 Changes in Lower Income Countries. *Bull. Am. Meteorol. Soc.* 101, E1851–E1860.
 1115 <https://doi.org/10.1175/BAMS-D-19-0317.1>
 1116 Patricola, C.M., Wehner, M.F., 2018. Anthropogenic influences on major tropical cyclone
 1117 events. *Nature* 563, 339–346. <https://doi.org/10.1038/s41586-018-0673-2>
 1118 Pekel, J.-F., Cottam, A., Gorelick, N., Belward, A.S., 2016. High-resolution mapping of global

1119 surface water and its long-term changes. *Nature* 540, 418–422.
1120 <https://doi.org/10.1038/nature20584>

1121 Probst, P., Annunziato, A., 2019. Tropical Cyclone IDAI: analysis of the wind, rainfall and
1122 storm surge impact. Joint Research Centre (EUROPEAN COMMISSION). URL:
1123 [https://www.humanitarianresponse.info/sites/www.humanitarianresponse.info/files/do](https://www.humanitarianresponse.info/sites/www.humanitarianresponse.info/files/documents/files/joint_research_centre_analysis_of_wind_rainfall_and_storm_surge_impact_09_april_2019.pdf)
1124 [cuments/files/joint_research_centre_analysis_of_wind_rainfall_and_storm_surge_im](https://www.humanitarianresponse.info/sites/www.humanitarianresponse.info/files/documents/files/joint_research_centre_analysis_of_wind_rainfall_and_storm_surge_impact_09_april_2019.pdf)
1125 [pact_09_april_2019.pdf](https://www.humanitarianresponse.info/sites/www.humanitarianresponse.info/files/documents/files/joint_research_centre_analysis_of_wind_rainfall_and_storm_surge_impact_09_april_2019.pdf).

1126 ReliefWeb, 2019a. Mozambique: Cyclone Idai & Floods Flash Update No. 10, 26 March
1127 2019. URL: [https://reliefweb.int/report/mozambique/mozambique-cyclone-idai-floods-](https://reliefweb.int/report/mozambique/mozambique-cyclone-idai-floods-flash-update-no-10-26-march-2019)
1128 [flash-update-no-10-26-march-2019](https://reliefweb.int/report/mozambique/mozambique-cyclone-idai-floods-flash-update-no-10-26-march-2019). Accessed on 2023-05-15.

1129 ReliefWeb, 2019b. 'The First City Completely Devastated by Climate Change' Tries to
1130 Rebuild after Cyclone Idai. URL: [https://reliefweb.int/report/mozambique/first-city-](https://reliefweb.int/report/mozambique/first-city-completely-devastated-climate-change-tries-rebuild-after-cyclone-idai)
1131 [completely-devastated-climate-change-tries-rebuild-after-cyclone-idai](https://reliefweb.int/report/mozambique/first-city-completely-devastated-climate-change-tries-rebuild-after-cyclone-idai).

1132 Resio, D.T., Irish, J.L., 2016. Tropical Cyclone Storm Surge Risk, in: *Handbook of Coastal*
1133 *and Ocean Engineering*. WORLD SCIENTIFIC, pp. 1405–1422.
1134 https://doi.org/10.1142/9789813204027_0049

1135 Riahi, K., van Vuuren, D.P., Kriegler, E., Edmonds, J., O'Neill, B.C., Fujimori, S., Bauer, N.,
1136 Calvin, K., Dellink, R., Fricko, O., Lutz, W., Popp, A., Cuaresma, J.C., Kc, S.,
1137 Leimbach, M., Jiang, L., Kram, T., Rao, S., Emmerling, J., Ebi, K., Hasegawa, T.,
1138 Havlik, P., Humpenöder, F., Da Silva, L.A., Smith, S., Stehfest, E., Bosetti, V., Eom,
1139 J., Gernaat, D., Masui, T., Rogelj, J., Strefler, J., Drouet, L., Krey, V., Luderer, G.,
1140 Harmsen, M., Takahashi, K., Baumstark, L., Doelman, J.C., Kainuma, M., Klimont,
1141 Z., Marangoni, G., Lotze-Campen, H., Obersteiner, M., Tabeau, A., Tavoni, M., 2017.
1142 The Shared Socioeconomic Pathways and their energy, land use, and greenhouse
1143 gas emissions implications: An overview. *Glob. Environ. Change* 42, 153–168.
1144 <https://doi.org/10.1016/j.gloenvcha.2016.05.009>

1145 Sauer, I.J., Reese, R., Otto, C., Geiger, T., Willner, S.N., Guillod, B.P., Bresch, D.N., Frieler,
1146 K., 2021. Climate signals in river flood damages emerge under sound regional
1147 disaggregation. *Nat. Commun.* 12, 2128. [https://doi.org/10.1038/s41467-021-22153-](https://doi.org/10.1038/s41467-021-22153-9)
1148 [9](https://doi.org/10.1038/s41467-021-22153-9)

1149 Scherrer, S.C., Fischer, E.M., Posselt, R., Liniger, M.A., Croci-Maspoli, M., Knutti, R., 2016.
1150 Emerging trends in heavy precipitation and hot temperature extremes in Switzerland.
1151 *J. Geophys. Res. Atmospheres* 121, 2626–2637.
1152 <https://doi.org/10.1002/2015JD024634>

1153 Schiavina, M., Freire, S., MacManus, K., 2019. GHS population grid multitemporal (1975,
1154 1990, 2000, 2015) R2019A. European Commission, Joint Research Centre (JRC).
1155 <https://doi.org/10.2905/42E8BE89-54FF-464E-BE7B-BF9E64DA5218>

1156 Shen, X., Wang, D., Mao, K., Anagnostou, E., Hong, Y., 2019. Inundation Extent Mapping by
1157 Synthetic Aperture Radar: A Review. *Remote Sens.* 11, 879.
1158 <https://doi.org/10.3390/rs11070879>

1159 Shepherd, T.G., 2016. A Common Framework for Approaches to Extreme Event Attribution.
1160 *Curr. Clim. Change Rep.* 2, 28–38. <https://doi.org/10.1007/s40641-016-0033-y>

1161 Shepherd, T.G., Boyd, E., Calel, R.A., Chapman, S.C., Dessai, S., Dima-West, I.M., Fowler,
1162 H.J., James, R., Maraun, D., Martius, O., Senior, C.A., Sobel, A.H., Stainforth, D.A.,
1163 Tett, S.F.B., Trenberth, K.E., van den Hurk, B.J.J.M., Watkins, N.W., Wilby, R.L.,
1164 Zenghelis, D.A., 2018. Storylines: an alternative approach to representing uncertainty
1165 in physical aspects of climate change. *Clim. Change* 151, 555–571.
1166 <https://doi.org/10.1007/s10584-018-2317-9>

1167 Strauss, B.H., Orton, P.M., Bittermann, K., Buchanan, M.K., Gilford, D.M., Kopp, R.E., Kulp,
1168 S., Massey, C., Moel, H. de, Vinogradov, S., 2021. Economic damages from
1169 Hurricane Sandy attributable to sea level rise caused by anthropogenic climate
1170 change. *Nat. Commun.* 12, 2720. <https://doi.org/10.1038/s41467-021-22838-1>

1171 Takayabu, I., Hibino, K., Sasaki, H., Shiogama, H., Mori, N., Shibutani, Y., Takemi, T., 2015.
1172 Climate change effects on the worst-case storm surge: a case study of Typhoon
1173 Haiyan. *Environ. Res. Lett.* 10, 064011. [27](https://doi.org/10.1088/1748-</p>
</div>
<div data-bbox=)

1174 9326/10/6/064011
 1175 The World Bank, 2022. World Development Indicators. Population, total - Mozambique.
 1176 Tozer, B., Sandwell, D.T., Smith, W.H.F., Olson, C., Beale, J.R., Wessel, P., 2019. Global
 1177 Bathymetry and Topography at 15 Arc Sec: SRTM15+. *Earth Space Sci.* 6, 1847–
 1178 1864. <https://doi.org/10.1029/2019EA000658>
 1179 Trenberth, K.E., Fasullo, J.T., Shepherd, T.G., 2015. Attribution of climate extreme events.
 1180 *Nat. Clim. Change* 5, 725–730. <https://doi.org/10.1038/nclimate2657>
 1181 UK Government Office for Science, 2011. Foresight: Migration and Global Environmental
 1182 Change (2011). Final Project Report [WWW Document]. GOV.UK. URL
 1183 [https://www.gov.uk/government/publications/migration-and-global-environmental-](https://www.gov.uk/government/publications/migration-and-global-environmental-change-future-challenges-and-opportunities)
 1184 [change-future-challenges-and-opportunities](https://www.gov.uk/government/publications/migration-and-global-environmental-change-future-challenges-and-opportunities) (accessed 1.4.23).
 1185 van Berchum, E.C., van Ledden, M., Timmermans, J.S., Kwakkel, J.H., Jonkman, S.N.,
 1186 2020. Rapid flood risk screening model for compound flood events in Beira,
 1187 Mozambique. *Nat. Hazards Earth Syst. Sci.* 20, 2633–2646.
 1188 <https://doi.org/10.5194/nhess-20-2633-2020>
 1189 van den Hurk, B.J.J.M., Baldissera Pacchetti, M., Boere, E., Ciullo, A., Coulter, L., Dessai,
 1190 S., Ercin, E., Goulart, H., Hamed, R., Hochrainer-Stigler, S., Koks, E., Kubiczek, P.,
 1191 Levermann, A., Mechler, R., van Meersbergen, M., Mester, B., Middelani, R.,
 1192 Minderhoud, K., Mysiak, J., Nirandjan, S., van den Oord, G., Otto, C., Sayers, P.,
 1193 Schewe, J., Shepherd, T.G., Sillmann, J., Stuparu, D., Vogt, T., Witpas, K., 2023.
 1194 Climate impact storylines for assessing socio-economic responses to remote events.
 1195 *Clim. Risk Manag.* 100500. <https://doi.org/10.1016/j.crm.2023.100500>
 1196 van Oldenborgh, G.J., van der Wiel, K., Kew, S., Philip, S., Otto, F., Vautard, R., King, A.,
 1197 Lott, F., Arrighi, J., Singh, R., van Aalst, M., 2021. Pathways and pitfalls in extreme
 1198 event attribution. *Clim. Change* 166, 13. <https://doi.org/10.1007/s10584-021-03071-7>
 1199 Warren, M., 2019. Why Cyclone Idai is one of the Southern Hemisphere's most devastating
 1200 storms. *Nature*. <https://doi.org/10.1038/d41586-019-00981-6>
 1201 Webster, P.J., Holland, G.J., Curry, J.A., Chang, H.-R., 2005. Changes in Tropical Cyclone
 1202 Number, Duration, and Intensity in a Warming Environment. *Science* 309, 1844–
 1203 1846. <https://doi.org/10.1126/science.1116448>
 1204 Wessel, P., Smith, W., 1996. A global, self-consistent, hierarchical, high-resolution shoreline
 1205 database. *J. Geophys. Res.* 101, 8741–8743. <https://doi.org/10.1029/96JB00104>
 1206 Wulder, M.A., White, J.C., Loveland, T.R., Woodcock, C.E., Belward, A.S., Cohen, W.B.,
 1207 Fosnight, E.A., Shaw, J., Masek, J.G., Roy, D.P., 2016. The global Landsat archive:
 1208 Status, consolidation, and direction. *Remote Sens. Environ.* 185, 271–283.
 1209 Yamazaki, D., Ikeshima, D., Sosa, J., Bates, P.D., Allen, G.H., Pavelsky, T.M., 2019. MERIT
 1210 Hydro: A High-Resolution Global Hydrography Map Based on Latest Topography
 1211 Dataset. *Water Resour. Res.* 55, 5053–5073. <https://doi.org/10.1029/2019WR024873>
 1212 Zscheischler, J., Martius, O., Westra, S., Bevacqua, E., Raymond, C., Horton, R.M., van den
 1213 Hurk, B., AghaKouchak, A., Jézéquel, A., Mahecha, M.D., Maraun, D., Ramos, A.M.,
 1214 Ridder, N.N., Thiery, W., Vignotto, E., 2020. A typology of compound weather and
 1215 climate events. *Nat. Rev. Earth Environ.* 1, 333–347. [https://doi.org/10.1038/s43017-](https://doi.org/10.1038/s43017-020-0060-z)
 1216 [020-0060-z](https://doi.org/10.1038/s43017-020-0060-z)
 1217
 1218
 1219